DEPARTMENT OF PHYSICS
UNIVERSITY OF JYVÄSKYLÄ
RESEARCH REPORT No. 1/2003

SCALING AND NOISE IN SLOW COMBUSTION OF PAPER

BY
JUSSI MAUNUKSELA

Academic Dissertation
for the Degree of
Doctor of Philosophy

To be presented, by permission of the
Faculty of Mathematics and Science
of the University of Jyväskylä,
for public examination in Auditorium FYS-1 of the
University of Jyväskylä on 28. March 2003
at 12 o'clock

Jyväskylä, Finland
March, 2003

ISBN 978-951-39-3139-1

URN:ISBN:978-951-39-3139-1

Preface

The foundation of this work was laid out between summers 1995-7 with the designing, construction, and testing of the experimental setup, used in this work, as part of my Master's Thesis co-authored with Mr. Markko Myllys. The experimental and analytical work reviewed in this Thesis has been carried out during the years 1997-2003 at the Department of Physics in the University of Jyväskylä in collaboration with Mr. Markko Myllys, Docent Juha Merikoski, and Professor Jussi Timonen, and with Docent Mikko Alava and Professor Tapio Ala-Nissilä from Helsinki University of Technology. Also the contribution of Dr. Olli-Pekka Kähkönen and Dr. Nikolas Provatas to this research at the Master's Thesis phase should be noted. The determination of the stochastic evolution equation from experimental data was done in collaboration with Professor Tommi Kärkkäinen from the University of Jyväskylä, and with Mr. Marco Welling and Dr. Rinke Wijngaarden from the Vrije Universiteit, Amsterdam. The work has been supervised by Professor Jussi Timonen and Docent Juha Merikoski.

First and foremost I would like to express my gratitude to my co-worker Mr. Markko Myllys. Without his invaluable contribution this research may never have taken off. I am also grateful to my supervisors Professor Jussi Timonen and Docent Juha Merikoski for their invaluable critique and contributions during the preparation of my enclosed articles and, especially, this Thesis. I also wish to thank Docent Alava and Professor Ala-Nissilä for their contributions during the preparation of the enclosed articles. I am grateful also to the current and former inhabitants of FL348 and to the staff of the Department of Physics for the great working conditions they have provided for my graduate studies. The financial support from the International PhD Programme in Pulp and Paper Science and Technology (PaPSaT) and the University of Jyväskylä is gratefully acknowledged.

Finally, I want to thank my parents and siblings for their support during this work.

Jyväskylä, March 2003

Jussi Maunuksela

Abstract

Maunuksela, Jussi
Scaling and Noise in Slow Combustion of Paper
Jyväskylä: University of Jyväskylä, 2003, 114 p.
(Research report/Department of Physics, University of Jyväskylä,
ISSN 0075-465X; 1/2003)
ISBN 951-39-1462-3
diss.

Theory of non-equilibrium interface dynamics is well developed but experiments often do not conform with theoretical predictions. The main purpose of the work reviewed in this Thesis is to demonstrate in detail that asymptotically the scaling behaviour of slow-combustion fronts is consistent with that of the Kardar-Parisi-Zhang (KPZ) equation with uncorrelated noise. This is achieved by determining the scaling exponents, universal amplitude ratios, and the scaling function of the local interface width from the experimental data. Results are also obtained for the persistence properties of front-height fluctuations. Asymptotically temporal and spatial first-return properties follow the theoretical expectations for the stationary state, but the stationary short-range and transient behaviour of the fronts is found to be non-Markovian. Estimates for all the parameters of the KPZ equation are obtained by an inverse method and from the slope-dependent local velocity of the fronts. The observed short-range behaviour is shown to originate from the effective correlated noise, which consists of structural and dynamical contributions.

Keywords slow combustion, scaling, noise, KPZ equation, non-equilibrium phenomena

Author's address Jussi Maunuksela
Department of Physics
University of Jyväskylä
Finland

Supervisors Professor Jussi Timonen
Department of Physics
University of Jyväskylä
Finland

Docent Juha Merikoski
Department of Physics
University of Jyväskylä
Finland

Reviewers Professor Luis A. Nunes Amaral
Department of Chemical Engineering
Northwestern University
USA

Professor Preben Alstrøm
Niels Bohr Institute
Denmark

Opponent Professor Joachim Krug
Department of Theoretical Physics
University of Essen
Germany

List of Publications

A.I. MAUNUKSELA, J., MYLLYS, M., KÄHKÖNEN, O.-P., TIMONEN, J., PROVATAS, N., ALAVA, M. J., AND ALA-NISSILA, T., *Kinetic Roughening in Slow Combustion of Paper*. Phys. Rev. Lett. **79** (1997) 1515–1518.

A.II. MAUNUKSELA, J., MYLLYS, M., TIMONEN, J., KUITTU, M., ALA-NISSILA, T., ALAVA, M. J., AND PROVATAS, N., *Reply to the Comment of Amaral and Makse*. Phys. Rev. Lett. **80** (1998) 5707.

A.III. MAUNUKSELA, J., MYLLYS, M., TIMONEN, J., ALAVA, M.J., AND ALA-NISSILA, T., *Kardar-Parisi-Zhang Scaling in Kinetic Roughening of Fire Fronts*. Physica A **266** (1999) 372–376.

A.IV. MYLLYS, M., MAUNUKSELA, J., ALAVA, M.J., ALA-NISSILA, T., AND TIMONEN, J., *Scaling and Noise in Slow Combustion of Paper*. *Phys. Rev. Lett.* ***84*** *(2000) 1946–1949*.

A.V. MYLLYS, M., MAUNUKSELA, J., ALAVA, M., ALA-NISSILA, A., MERIKOSKI, J., AND TIMONEN, J., *Kinetic Roughening in Slow Combustion of Paper*. Phys. Rev. E **64** (2001) 036101.

A.VI. MERIKOSKI, J., MAUNUKSELA, J., MYLLYS, M., TIMONEN, J., AND ALAVA, M. J., *Temporal and Spatial Persistence of Combustion Fronts*. Phys. Rev. Lett. **90** (2003) 024501.

A.VII. MAUNUKSELA, J., MYLLYS, M., MERIKOSKI, J., TIMONEN, J., KÄRKKÄINEN, T., WELLING, M. S., AND WIJNGAARDEN, R. J., *Determination of the Stochastic Evolution Equation from Noisy Experimental Data*. To appear in Eur. Phys. J. B.

The author of this thesis has been involved in the design, testing and operation of the experimental equipment, and in the analysis of the collected data. Majority of the results presented in this thesis are reported in the enclosed articles in Appendices A.I–A.VII. The author of this Thesis has written the first draft of the article A.VII, and selected parts of the articles A.IV–A.VI. The author has performed almost all of the numerical analysis and produced the graphics for the articles.

Contents

Preface i

Abstract iii

List of Publications v

1 Introduction 1

2 Analysis of Scaling Properties of Interfaces 3
2.1 Height-height correlation function . . . 3
2.2 Structure factor . . . 6
2.3 Interface width . . . 6
2.4 First-return distributions . . . 8

3 Langevin Equation 11
3.1 Edwards-Wilkinson (EW) equation . . . 11
3.2 Kardar-Parisi-Zhang (KPZ) equation . . . 12
3.3 Annealed and quenched noise . . . 12
3.4 KPZ model parameters I . . . 14
3.4.1 λ from the local velocity . . . 14
3.4.2 D/ν from the equal time correlation functions . . . 15
3.4.3 Universal (dimensionless) quantities . . . 15
3.5 KPZ model parameters II . . . 16
3.5.1 Inverse method . . . 17
3.5.2 Pseudo-spectral method . . . 18

4 Experiments and Data 21

5 Filtering of Erratic Noise 25

6 Results and Discussion 27
6.1 Scaling of correlation functions and front width . . . 27
6.1.1 Crossover behaviour . . . 27
6.1.2 Kardar-Parisi-Zhang scaling . . . 28
6.1.3 Anomalous scaling . . . 31
6.2 Scaling and noise . . . 32
6.3 Persistence . . . 34
6.4 Model parameters . . . 35
6.4.1 Amplitudes, dimensionless constants and λ . . . 35
6.4.2 KPZ and its parameters by inversion from observed fronts . . . 36

7 Conclusions 41

Chapter 1

Introduction

This thesis is devoted to an experiment-based survey and analysis of dynamics and kinetic roughening of interfaces propagating in a random medium. Kinetic roughening of moving interfaces is a ubiquitous phenomenon in nature, ranging from surface growth to propagation of various kinds of fronts in random media. The term kinetic roughening implies a process by which the noisy local displacement dynamics of an interface is transformed into scale-invariant fluctuations of the interface position. Extensive theoretical work during the last decade and a half has led to a classification of these phenomena according to the asymptotic behaviour of the scaling properties of various quantities such as surface roughness. This classification, in many cases, can also be obtained by identifying the interface dynamics with that of an appropriate Langevin equation. In practice the effective noise may have system specific correlations and/or an anomalous magnitude distribution, which both affect the scaling behaviour.

The position of an interface is assumed to be described by a single-valued function $h = h(x,t)$. If this function remains unchanged upon anisotropic rescaling by an arbitrary factor λ, $h(x,t) \simeq \lambda^{-\chi} h(\lambda x, \lambda^z t)$, the interface is called *self-affine*. Here "$\simeq$" implies equivalent *statistical* properties. The scaling properties of fluctuations in the interface position (height) can be analysed *e.g.* via the height-height correlation function (see Section 2.1 below) of the interface. For self-affine interfaces this correlation function is also invariant upon similar rescaling, $C_q(r,t) \simeq \lambda^{-\chi} C_q(\lambda r, \lambda^z t)$, with χ between zero and one. These exponents, χ and z, correspond to stationary and 'dynamic' scaling of the interface fluctuations, respectively.

The theory of (non-equilibrium) interface dynamics was well developed by the mid 1990's, and had produced a detailed description of various scaling properties and fluctuation distributions of especially one-dimensional interfaces, but experiments did not typically conform with theoretical predictions [71,26,9,52]. The measured one-dimensional interfaces included those of fluid penetrating into a porous medium [66,28,30], growing bacterial colonies [72], and advancing slow-combustion fronts in paper [74]. Later measurements were also done on magnetic flux fronts

penetrating a high-T_c thin-film superconductor [69].

Although the kinetically roughened interfaces appeared to be self-affine in each of these systems, their behaviour was 'anomalous', at least at small length scales, such that the measured roughness exponent typically exceeded the KPZ value for one-dimensional interfaces, $\chi = 1/2$ (assuming uncorrelated Gaussian noise). Experiments *e.g.* on fluid penetration into a porous medium [66,28,30], mostly yielded a roughness exponent χ that varied in a wide range $0.65 - 0.91$, except for the one reported in Ref. [30] for the asymptotic behaviour at long length scales, $\chi \simeq 0.49$. In [30] the temporal scaling of the interface was also determined with the result $\beta \simeq 0.65$ for the growth exponent. This was the first reported measurement of the growth exponent, and the result also exceeded the KPZ value $\beta = 1/3$.

The unexplained variation in the measured scaling exponents, their deviation typically from the KPZ values, and the fact that only the roughness exponent had usually been measured, were the main motivations of the present work: We wanted to measure all scaling exponents for one system, with statistics enough for reliable averaging, and to probe its true scaling behaviour in more detail by measuring also its various fluctuation distributions. For the system to be studied we chose the flameless burning of a random two-dimensional medium, easily realised by slow combustion of sheets of paper. Zhang *et al.* [74] had already performed one such experiment, but they had estimated only the roughness exponent with a result well above the KPZ value. In this experiment only one front was however determined for each sample, so averaging over noise could not be very extensive.

In our experiments sheets of paper were positioned inside a combustion chamber and ignited at one end with a heating wire stretched over the sample. The propagation of the slow-combustion front thus produced was then recorded with a CCD-camera system and stored in digital form. This made it possible for us to study the time- and space-dependent behaviour of the combustion fronts in great detail, and with good statistics. For copier-paper burns *e.g.*, results can be given as averages over up to about 40 000 individual fronts.

Chapter 2

Analysis of Scaling Properties of Interfaces

Typically, late stages of growth processes are characterised by generic scale invariance of the relevant correlation functions, which is reflected in their power-law behaviours in both space and time. Since the corresponding scaling exponents do not usually depend on the microscopic details of the system under investigation, but only reflect its underlying symmetries, growth processes are often divided into kinetic universality classes according to the values of these characteristic exponents [9,52,68]. Likewise this scale invariance is reflected in the universal scaling forms for correlation functions, interface width, and various fluctuation distributions [9, 52].

In this chapter we thus give a short introduction to the analysis tools employed here in the determination of scaling exponents and scaling functions: height-height correlation functions, structure factor, interface width, and first-return distributions.

2.1 Height-height correlation function

Scaling exponents can be determined by analysing the scaling behaviour of correlation functions such as the *height-height correlation function* [52]

$$\begin{aligned} G(r,t) &= \left\langle [\delta h(r+x,t) - \delta h(x,t)]^2 \right\rangle \\ &\equiv r^{2\chi} g(r/\xi(t)), \end{aligned} \tag{2.1}$$

where $\delta h(x,t) \equiv h(x,t) - \overline{h}$ is height fluctuation of a moving interface (or front) above point x on a baseline of dimension $d = 1$, $\overline{h}(t)$ is the average height of the front of length L (the width of the system under investigation), and $\langle \cdot \rangle$ an average over all fronts. The roughness exponent χ characterises the saturated regime, in which the horizontal correlation length $\xi(t) \sim t^{1/z}$ (z is the so called dynamic exponent) has reached a value larger than the system size L. The behaviour of the scaling function $g(x)$ is correspondingly divided into two regimes by the value of the correlation

length such that

$$g(x) \sim \begin{cases} x^{-2\chi} & \text{for } x \gg 1 \\ \text{const} & \text{for } x \ll 1 \end{cases} . \tag{2.2}$$

For the interface heights $h(x,t)$, we can also consider the q'th order height-height correlation functions

$$C_q(r,\tau) = \langle [\delta h(x,t) - \delta h(x+r,t+\tau)]^q \rangle_{x,t} , \tag{2.3}$$

where $\langle \cdot \rangle_{x,t}$ denotes average over all fronts. In the stationary state we define [53,11, 10,8,57]

$$G_q(r) \equiv C_q(r,0) \sim r^{q\chi_q} , \tag{2.4}$$

and

$$C_q(\tau) \equiv C_q(0,\tau) \sim \tau^{q\beta_q} , \tag{2.5}$$

which can be used to extract estimates for the roughness and growth exponents χ_q and β_q, respectively. Note that in the q'th order height-height correlation functions as defined in Eq. (2.3), q is both positive and even. For interfaces that obey the KPZ equation with Gaussian noise (see Section 3.2), Eqs. (2.4) and (2.5) give constant $\chi_q =: \chi$ and $\beta_q =: \beta$. Figure 2.1 displays the spatial and temporal height-height correlation functions $C_q(r,\tau)$ with $q = 2$ for three sets of experimental data. The q'th order correlation functions are said to exhibit a nontrivial *multiscaling* behaviour if *e.g.* χ_q varies continuously with q at least for some region of the q values [11]. It has been suggested that interfaces generated by models (see *e.g.* Ref. [75]) with large-rare-events dominated roughening are examples of this *'multiaffine'* scaling, and require an infinite family of exponents for a full description of their scaling behaviour [8].

We determined the scaling region, the scaling exponents χ and β, and their accuracy, by using *running exponents* determined *e.g.* from Eq. (2.4). (A variant of this approach is to use consecutive slopes [9].) The *running exponent* is defined as

$$\chi_{\text{eff}}(r) = \frac{1}{q} \frac{\log_{10}[G_q(r')/G_q(r)]}{\log_{10}(r'/r)} , \tag{2.6}$$

where a convenient choice for r' is *e.g.* $r' = 4r$. By plotting the running exponent as a function of the length scale r, we obtained an estimate for the scaling region, where $\chi_{\text{eff}}(r) \simeq \text{const}$. The scaling exponent χ was then determined by performing a linear least-squares analysis of *e.g.* $\log_{10} G_q(r) = q\chi_q \log_{10} r + \text{const}$ in the scaling region, and the accuracy of the scaling exponent was estimated as the standard deviation of the running exponent $\chi_{\text{eff}}(r)$ from χ in the scaling region.

Accidental inhomogeneities and short-range correlated noise in the data will cause non-zero offsets at the origin in the correlation functions, and they complicate accurate determination of possible scaling exponents. In order to get rid of these

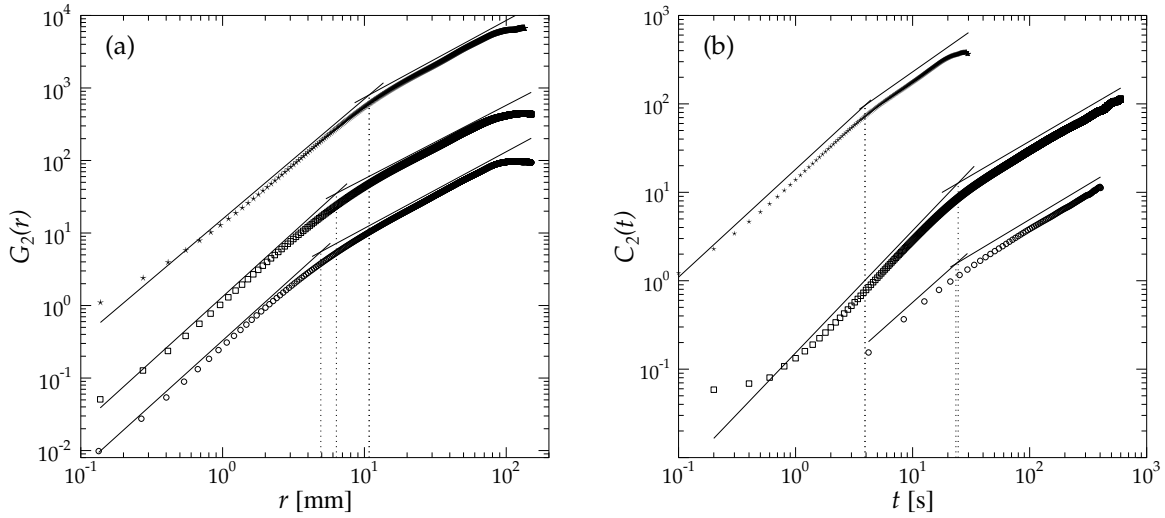

FIGURE 2.1 The (a) spatial and (b) temporal height-height correlation functions $G_2(r)$ and $C_2(t)$, respectively. The results are averages over 10 of the $70\,\mathrm{g/m^2}$ (○) and 6 of the $80\,\mathrm{g/m^2}$ (□) copier paper burns, and 32 of the $9.1\,\mathrm{g/m^2}$ lens paper burns (★). The crossover scales r_c and t_c are shown by dotted vertical lines, and the solid lines indicate slopes that correspond to the exponents shown in Tables 6.1 and 6.2.

(supposedly) additive constant factors in the correlation functions, we performed linear least-squares analysis of *e.g.* $\log_{10}\left[G_q(2r) - G_q(r)\right] = q\chi_q \log_{10}(r) + \mathrm{const}$, in the same spirit as how the 'intrinsic' width is removed from the interface width (see Section 2.3 below).

Since the correlation functions are calculated in the stationary state, a rough initial front line does not hamper the accurate determination of the scaling behaviour, especially the time-dependent scaling. On the contrary, in some experiments the stationary state was reached only because of rough ignition. Also, in practice the finite spatial resolution in the experimental data influences the observed scaling behaviour. Therefore, our preferred tool for the scaling analysis was the height-height correlation function Eq. (2.3), where corrections due to finite resolution can be neglected [12].

2.2 Structure factor

For the determination of scaling exponents we can also measure the power spectrum of the interface, *i.e.*, the *structure factor*, which is essentially the Fourier transform of the height-height correlation function, [68]

$$\begin{aligned} S(k,t) &= \langle \hat{h}(k,t)\hat{h}(-k,t)\rangle \quad \left(= \frac{1}{2}\sum_r (\delta_{k,0} - e^{ik\cdot r})G(r,t) \right) \\ &\equiv k^{-\gamma} s(k^z t), \end{aligned} \tag{2.7}$$

in which $\gamma = 2\chi + d$ and $\hat{h}(k,t) = L^{-1/2}\sum_x [h(x,t) - \overline{h}(t)]e^{ik\cdot x}$, with $\overline{h}(t)$ the spatial average of $h(x,t)$. In this case the asymptotics of the scaling function are [68]

$$s(x) \sim \begin{cases} x^{\gamma/z}, & \gamma > z \\ x, & \gamma \leq z \end{cases} \tag{2.8}$$

for $x \ll 1$, and

$$s(x) = \text{const} \quad \text{for } x \gg 1. \tag{2.9}$$

The limiting behaviour Eq. (2.8) follows from the fact that noise in the system is not renormalised for $\gamma \leq z$ as can be shown by power counting. Thus the k modes with $k < 2\pi/\xi(t)$ propagate in an uncorrelated fashion, $S(k,t) \sim tk^{z-\gamma}$. For $\gamma > z$ this is no longer possible since, in the limit $k \to 0$, $S(k,t)$ must not have a singularity at a finite time. Hence, noise is now renormalised, which happens *e.g.* in the Kardar-Parisi-Zhang equation [35].

The structure factor is sensitive to the global slope of the interface. The power spectrum of a linear ramp has slope -2, which is also the slope ($-\gamma = -2\chi - 1$) of the power spectrum of a one-dimensional self-affine interface with roughness exponent $\chi = 1/2$ [67]. Also, density of points is low in the asymptotic region (small k) of the (discrete) structure factor, in which we expect to find the KPZ behaviour. Therefore we did not typically use the structure factor in our analysis of the scaling properties.

2.3 Interface width

Perhaps the most traditional approach to study the scaling behaviour of interfaces is to consider their width W defined as [68,21]

$$\begin{aligned} W^2(t,L) &\equiv L^{-1}\sum_x \langle [h(x,t) - \overline{h}(t)]^2 \rangle \\ &\equiv L^{-1}\sum_k S(k,t) \equiv \frac{1}{2L}\sum_r G(r,t)\,. \end{aligned} \tag{2.10}$$

Interface width satisfies the Family-Vicsek scaling relation [18]

$$W(t,L) \sim L^{\chi} f\left(\frac{t}{L^z}\right) \sim \begin{cases} t^{\beta} & \text{for} \quad \xi \ll L \\ L^{\chi} & \text{for} \quad \xi \gg L \end{cases} , \tag{2.11}$$

where the *correlation length* ξ is the characteristic distance over which the local heights are correlated. When an interface begins to propagate, ξ grows with time. When it reaches the size of the system L, the entire interface becomes correlated, which leads to saturation of the interface width. Thus at saturation $\xi \sim L$, and according to Eq. (2.11) this saturation occurs at a time $t_{\times} \sim L^z$. By replacing L with ξ, correlation length behaves as $\xi \sim t^{1/z}$ for $t \ll t_{\times}$.

An estimate for the roughness exponent χ can as well be obtained from the local interface width [52], defined as

$$w^2(\ell,t) = \left\langle \left\langle \left[h(x,t) - \langle h(x,t)\rangle_\ell\right]^2 \right\rangle_\ell \right\rangle = \left\langle \langle h^2(x,t)\rangle_\ell - \langle h(x,t)\rangle_\ell^2 \right\rangle , \tag{2.12}$$

where the notation $\langle\cdot\rangle_\ell$ denotes spatial averaging over a subsystem of size ℓ and $\langle\cdot\rangle$ over all subsystems of size ℓ in a system of total size L. In order to improve the estimates for the scaling exponents, the 'intrinsic' width of the interfaces should first be subtracted from the data in the spirit of the usual convolution ansatz [73, 36, 19]. For growing self-affine interfaces, the local width with intrinsic width subtracted also follows Eq. (2.11), which now takes the form [36]

$$w^2(\ell,t) - w_i^2 \sim \begin{cases} t^{2\beta} & \text{for } t \ll \ell^z \\ \ell^{2\chi} & \text{for } t \gg \ell^z \end{cases} , \tag{2.13}$$

and the intrinsic width can be subtracted by writing *e.g.*

$$w^2(\ell,2t) - w^2(\ell,t) = [a(2t)^{2\beta} + w_i^2] - [at^{2\beta} + w_i^2] \tag{2.14a}$$

$$= a(2^{2\beta} - 1)t^{2\beta} , \tag{2.14b}$$

where $t \ll \ell^z$ and a is independent of L. The scaling exponents can be determined by a simple linear least-squares analysis of $\log_{10}[w^2(2t) - w^2(t)] = 2\beta \log_{10} t + \text{const}$ in the scaling regime determined from the running exponent results (see Section 2.1) after the intrinsic width was subtracted. Figure 2.2 displays the local width $w(\ell)$ before and after the intrinsic width was subtracted and the running roughness exponent χ_{eff} calculated for three different paper grades.

The local width $w(\ell,t)$ allows, furthermore, for the determination of the scaling function related to that of Eq. (2.11) from experimental data. This can be done by plotting the quantity $w(\ell,t)/\ell^{\chi}$ against t/ℓ^z and observing the data collapse.

Interface width is not a particularly good quantity to determine the temporal scaling behaviour [Eqs. (2.10) and (2.11)] as, in the experiments, interfaces do not start as straight horizontal fronts. Also, it is difficult to get enough statistics as one

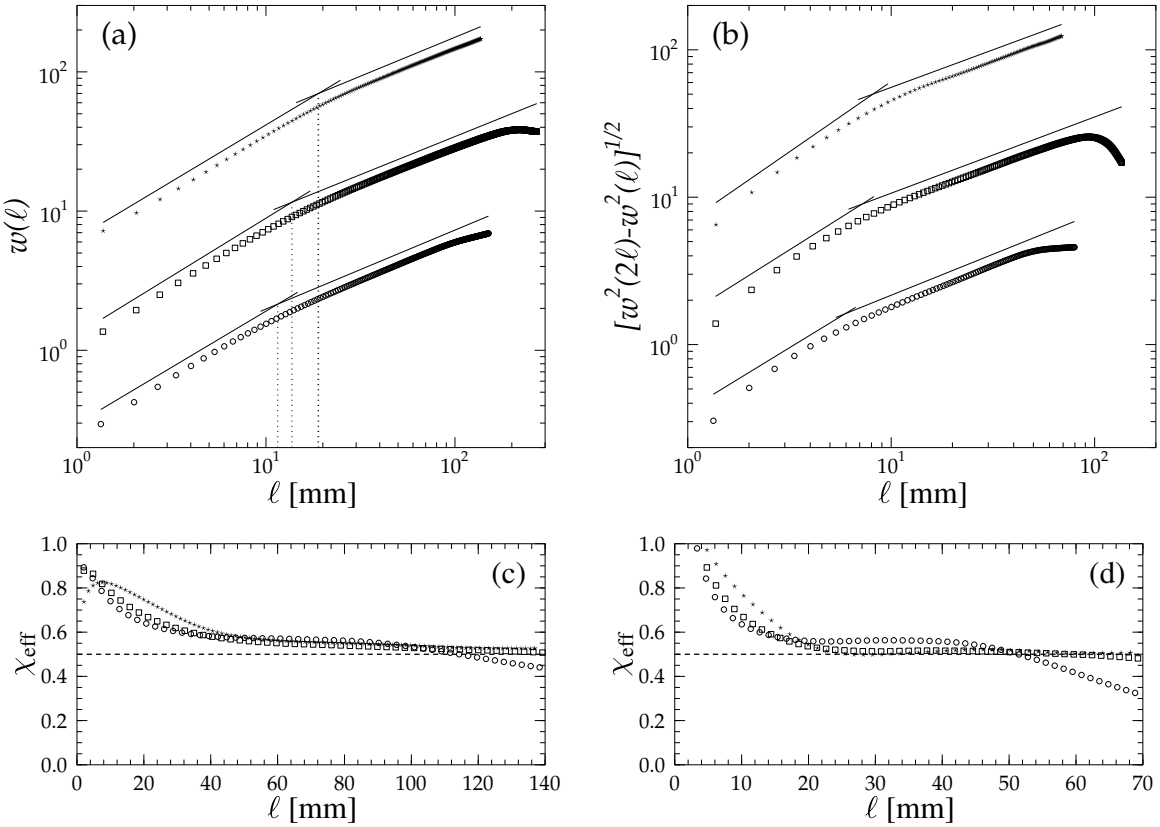

FIGURE 2.2 (a) The local width $w(\ell)$ calculated from 10 of the $70\,\mathrm{g/m^2}$ (○) and 6 of the $80\,\mathrm{g/m^2}$ (□) copier paper burns, and 32 of the $9.1\,\mathrm{g/m^2}$ lens paper burns (★), and (b) the local width with the intrinsic width subtracted. (a) The crossover lengths $\ell_c = 12(7),\ 14(6)$, and $18.8(4)\,\mathrm{mm}$ for these paper grades, respectively, are shown by the vertical dashed lines, and (a)-(b) the solid lines indicate slopes that correspond to the exponents in Tables 6.1 and 6.2. The running roughness exponents $\chi_{\rm eff}$ calculated from the local width before (c) and after (d) the intrinsic width was subtracted are also shown. The theoretical value $\chi = 1/2$ is indicated by the horizontal dashed line.

burn produces only one $W(t, L)$ curve. Therefore we did not typically use interface width in data analysis. On the other hand, the scaling properties of the local width Eq. (2.13) do not suffer from these shortcomings, and this quantity was regularly used to determine both β and χ.

2.4 First-return distributions

A particularly topical problem in non-equilibrium dynamics is *persistence*, which can be defined as the probability $P(t)$ that, at point x, a fluctuating non-equilibrium field $h(x, t)$ does not change sign up to time t [46, 44]. This probability may decay algebraically, $P(t) \sim t^{-\theta}$, in analogy with the scaling behaviours of the correlation

functions and interface width considered above, and thus defines a *persistence exponent* θ. In our case the non-equilibrium field is of course the local height fluctuation at time t of slow-combustion fronts.

Persistence can be analysed by considering the first-return distributions $f_{\pm}^{\mathrm{temp}}(\tau)$, *i.e.*, the distribution for return time τ, defined as the time the considered variable stays above $(+)$ or below $(-)$ a given reference level. The persistence exponents $\theta_{\pm}^{\mathrm{temp}}$ describe the decay of the related temporal persistence probabilities, and are defined via [39,45]

$$P_{\pm}^{\mathrm{temp}}(\tau) \sim \tau^{-\theta_{\pm}^{\mathrm{temp}}} , \tag{2.15}$$

where τ denotes the persistence time-scale. The temporal persistence probabilities [39] are related to the corresponding first-return distributions $f_{\pm}^{\mathrm{temp}}(\tau)$ via

$$P_{\pm}^{\mathrm{temp}}(\tau) \equiv P(\tau_{\pm} \geq \tau) = 1 - \int_{-\infty}^{\tau} f_{\pm}^{\mathrm{temp}}(\tau')\, d\tau' . \tag{2.16}$$

For general self-affine interfaces which need not be Gaussian [27,49], it can be shown that the temporal first-return distributions satisfy $f_{\pm}^{\mathrm{temp}}(\tau) \sim \tau^{-\theta_{\pm}^{\mathrm{temp}}-1}$, where for the KPZ equation the conjecture $\theta_{+}^{\mathrm{temp}} = \theta_{-}^{\mathrm{temp}} \equiv \theta_s = 1 - \beta$ is expected to hold in the stationary state [27,49,15,39].

One may likewise consider any particular front at a fixed time t and look at the interface profile as a stochastic process [45]. In analogy with the temporal case, the spatial persistence probabilities $P_{\pm}^{\mathrm{spat}}(\ell)$ that the interface stays above or below a given reference level, may have a power-law decay described by exponents $\theta_{\pm}^{\mathrm{spat}}$,

$$P_{\pm}^{\mathrm{spat}}(\ell) \sim \ell^{-\theta_{\pm}^{\mathrm{spat}}} . \tag{2.17}$$

Here ℓ denotes the persistence length scale and the persistence probability is related to the first-return distribution $f_{\pm}^{\mathrm{spat}}(\ell)$ via

$$P_{\pm}^{\mathrm{spat}}(\ell) \equiv P(\ell_{\pm} \geq \ell) = 1 - \int_{-\infty}^{\ell} f_{\pm}^{\mathrm{spat}}(\ell')\, d\ell' . \tag{2.18}$$

For the stationary state, the spatial persistence is expected to be related to the interface morphology via $\theta_{+}^{\mathrm{spat}} = \theta_{-}^{\mathrm{spat}} = 1 - \chi$.

In general, the temporal persistence behaviour can be characterised by considering the scaling functions of the general persistence probability $P(t_0, t)$, where t is measured beginning from time t_0 after the start of the kinetics from a flat initial profile [34]. Kallabis and Krug [34] observed, starting from a numerical growth model, that this has two limiting behaviours, the *transient behaviour* for t_0 before saturation and the *stationary-state behaviour* for t_0 after it, thus defining two persistence exponents. For the transient regime, Kallabis and Krug observed, *e.g.*, that persistence depends on the up-down asymmetry of the dynamics, in their model with values

1.2 and 1.6 for the transient temporal persistence exponents for fluctuations in the up and down directions, respectively [34].

In practice, *e.g*, the first-return times $\tau_\pm$ can be determined by following the fluctuations $\delta h(x,t)$ at a fixed point $x = x_0$ and time t, when the interface propagates with a finite average velocity v. For practical purposes we can then define the return times such that τ_+ is the length of the time interval between t_1 and t_2 with $\delta h(x_0,t_1) = 0 = \delta h(x_0,t_2)$, and $\delta h(x_0,t) > 0 \; \forall \; t \in]t_1,t_2[$. The return time τ_- is defined analogously for $\delta h(x_0,t) < 0$. For discrete sampling times the crossing times t_1 and t_2 can be determined by using linear interpolation: Find all t for which $\delta h(x,t) < 0 \leq \delta h(x,t+\Delta t)$ or $\delta h(x,t) > 0 \geq \delta h(x,t+\Delta t)$. The interpolated crossing times t_i are then determined as $t_i = t - \Delta t\,[\delta h(x,t)/(\delta h(x,t+\Delta t) - \delta h(x,t))]$, where Δt is the sampling time. The corresponding spatial quantities at fixed times are defined analogously.

In determining the first-return distributions, we measure the histogram of return times $\tau_\pm$. As explained in Ref. [47], in discrete time (and also in discrete space) sampling, one misses very short excursions, and correct normalisations of $P_\pm^{\mathrm{temp}}$ and $P_\pm^{\mathrm{spat}}$ are difficult. Therefore, we prefer to use the distributions $f_\pm^{\mathrm{temp}}$ and $f_\pm^{\mathrm{spat}}$, instead of their integrals, for determination of the persistence exponents (see Figure 6.4). In the limit of long time and length scales, the problems in these functions due to discrete sampling should disappear.

Chapter 3

Langevin Equation

Roughening behaviour can be classified by identifying the observed dynamics with that of a known Langevin equation. In this chapter we first (briefly) review results for two generic Langevin equations that are supposed to generally describe equilibrium and non-equilibrium interface dynamics. In the subsequent sections we then describe methods that can be used to identify the relevant parameters of the appropriate Langevin equation from experimental data.

3.1 Edwards-Wilkinson (EW) equation

The simplest linear equation describing the fluctuations of an equilibrium interface is a continuum partial differential equation first proposed by Edwards and Wilkinson [16] in their attempt to understand the inherently probabilistic process of particle sedimentation within a liquid. The Edwards-Wilkinson (EW) equation is given by

$$\frac{\partial h}{\partial t} = \nu \nabla^2 h + \eta \ , \tag{3.1}$$

for the height $h(x,t)$ of the sedimented layer. Here ν is called a 'surface tension' due to the tendency of the $\nu\nabla^2 h$ term to smooth the interface. The noise $\eta \equiv \eta(x,t)$ is assumed to be spatially and temporally uncorrelated and Gaussian, described by

$$\langle \eta(x,t) \rangle = 0, \tag{3.2}$$

$$\langle \eta(x,t)\eta(x',t') \rangle = 2D\delta(x-x')\delta(t-t') \ . \tag{3.3}$$

The fluctuations of the *equilibrium* interface described by the EW equation Eq. (3.1) are around $\langle h \rangle = \text{const}$, *i.e.*, neither of the two domains separated by the equilibrium interface grows at the expense of the other. A review of the properties of the EW equation and of the linear interface theory more generally can be found *e.g.* in Ref. [9].

3.2 Kardar-Parisi-Zhang (KPZ) equation

Kardar, Parisi and Zhang proposed a generic model for the evolution of the height of a *growing* interface in Ref. [35]. The simplest nonlinear Langevin equation in $1+1$ dimensions for the local growth of this height in a moving coordinate system for which $\langle h(x,t)\rangle = 0$, such that it is invariant under the transformation

$$h \to h + \varepsilon x, \quad x \to x + b\,\varepsilon t\ , \tag{3.4}$$

is given by

$$\frac{\partial h}{\partial t} = \nu\nabla^2 h + \frac{\lambda}{2}(\nabla h)^2 + \eta\ . \tag{3.5}$$

The transformation Eq. (3.4) corresponds to tilting of the interface by a small angle. Random fluctuations of the height, represented by $\eta \equiv \eta(x,t)$, are again taken to be Gaussian white noise described by Eqs. (3.2) and (3.3).

The physical origin of the nonlinear term in Eq. (3.5) is [26] in the local propagation (driving) of the interface along the outward normal. When this driving is projected onto the vertical axis, we find that the effective advance is proportional to

$$\sqrt{1+(\nabla h)^2}\ \approx\ 1 + \frac{1}{2}(\nabla h)^2 - \frac{1}{8}(\nabla h)^4 + \frac{1}{16}(\nabla h)^6 - \dots\ , \tag{3.6}$$

when $(\nabla h)^2$ is assumed small.

Due to a Galilean invariance [35, 54], invariance under the transformation Eq. (3.4) above, the exponents χ and $z\,(\equiv \chi/\beta)$ are linked by an identity $\chi + z = 2$. In $1+1$ dimensions ($d = 1$), Eq. (3.5) also satisfies a fluctuation-dissipation theorem [14] (FDT), from which one can obtain exactly that $\chi = \frac{1}{2}$. In this $d = 1$ case it is in fact possible to solve exactly all scaling exponents [25,24] and some of the scaling functions [61,62].

3.3 Annealed and quenched noise

The character of the noise η in Eqs. (3.1) and (3.5) has a major influence on the scaling exponents (see Table 3.1). There are two main types of noise discussed in literature [26,9]: (i) "thermal" or "annealed" depending on time such that $\eta = \eta(x,t)$ and (ii) "quenched" depending on time only via the position such that $\eta = \eta(x, h(x,t))$.

If the noise is *quenched*, a continuous motion of the interface requires application of a driving force F. There exists a critical force F_c below which, *i.e.*, for $F < F_c$, the interface will become *pinned* by the disorder after some finite time. For $F > F_c$, the interface moves indefinitely with an average velocity $v(F)$. At the depinning transition ($F = F_c$), it is sufficient to consider Eqs. (3.1) and (3.5) augmented with a driving force F and quenched disorder [4,9,26]. For $F \to F_c$, the moving interface is not self-affine and has effective exponents for short length and time scales; quenched

TABLE 3.1 Numerical estimates of the scaling exponents for one-dimensional interface roughening with annealed and quenched noise. For definitions of the symbols, see the related text below.

Model	χ	β	Reference
EW	$1/2$	$1/4$	[16]
KPZ	$1/2$	$1/3$	[35]
quenched EW			[4,70,42]
pinned $(F < F_c)$	≈ 1	≈ 0.88	
transition $(F \to F_c^+)$	≈ 0.92	≈ 0.86	
moving $(F \gg F_c)$	≈ 0.48	≈ 0.25	
quenched KPZ			[4,70,42]
pinned $(F < F_c)$	≈ 0.63	≈ 0.63	
transition $(F \to F_c^+)$	≈ 0.75	≈ 0.75	
moving $(F \gg F_c)$	≈ 0.50	≈ 0.30	
KPZ with power-law distributed noise			[75,38,13]
$\mu = 2 < \mu_c \approx 4$	1	1	
$\mu = 3 < \mu_c \approx 4$	$3/4$	$3/5$	
$\mu > \mu_c \approx 4$	$1/2$	$1/3$	
KPZ with spatially correlated noise			[54,26]
$1/4 \le \rho < 1$	$0.50 - 1.0$	$0.33 - 1.0$	
$\rho \to 0^+$	≈ 0.5	≈ 0.33	
KPZ with temporally correlated noise			[54,26]
$0.167 < \theta < 0.5$	$0.50 - 1.059$	$0.33 - 0.677$	
$\theta < 0.167$	$1/2$	$1/3$	

noise becomes asymptotically irrelevant and the annealed case is recovered.

The noise may also be uncorrelated but *distributed* by a power law instead of a Gaussian (we return to this problem in Section 6.2), or spatially and/or temporally correlated. The latter problem was investigated by Medina *et al.* in Ref. [54] by using the dynamic renormalization group method on the KPZ equation with the noise correlation [54]

$$\langle \eta(x,t)\eta(x',t') \rangle \sim |x-x'|^{2\rho-d}\,|t-t'|^{2\theta-1}\,, \tag{3.7}$$

where d is the dimension of the interface. If the noise is spatially correlated, *i.e.*, $\langle \eta(x,t)\eta(x',t') \rangle \sim |x-x'|^{2\rho-1}\delta(t-t')$, the scaling exponents obey the relation $\chi+z=2$, and are approximated by [26] $\chi = (1+2\rho)/3$, $\beta = (1+2\rho)/(5-2\rho)$ with $1/4 < \rho < 1$, while for $0 < \rho < 1/4$ the exponents have the values $\chi = 1/2$ and $\beta = 1/3$.

For the temporally correlated noise, *i.e.*, $\langle \eta(x,t)\eta(x',t') \rangle \sim \delta(x-x')|t-t'|^{2\theta-1}$ for a one-dimensional interface, Medina *et al.* [54] found that for $\theta < 0.167$ the situation becomes equivalent to that of short-range correlated noise with $\chi = 1/2$ and $\beta = 1/3$.

For $0.167 < \theta < 0.5$, the temporal correlations are relevant, and the exponents are approximated by $\chi(\theta) = 1.69\theta + 0.22$ and $\beta(\theta) = (1 + 2\theta)\chi(\theta)/(2\chi(\theta) + 1)$. For more details on this subject see *e.g.* the review by Halpin-Healy and Zhang [26].

3.4 KPZ model parameters I

3.4.1 λ from the local velocity

One way to measure c and λ (from experimental data) is based on the fact that interface velocity, in the length scale being considered, depends on the average tilt of the interface in that length scale. For an interface, whose dynamics is governed by the KPZ equation, Eq. (3.5), the average velocity v in scale l is given by

$$v = v_0 + \frac{\lambda}{l} \int_0^l d\mathbf{x} \sqrt{1 + (\nabla h)^2} \,, \tag{3.8}$$

where v_0 is the drift velocity due to external forces acting on the interface, and we have kept the full square root term in this expression. Assuming $(\nabla h)^2$ is small, the above expression can be expanded as usual so that

$$v \approx v_0 + \frac{\lambda}{l} \int_0^l d\mathbf{x} \left[1 + \frac{1}{2}(\nabla h)^2 - \frac{1}{8}(\nabla h)^4 + \ldots \right] \tag{3.9a}$$

$$= c + \frac{\lambda}{2l} \int_0^l d\mathbf{x} \, (\nabla h)^2 + \mathcal{O}\left[(\nabla h)^4\right] , \tag{3.9b}$$

where $c \equiv v_0 + \lambda$ is the zero-slope velocity.

If there is now a tilt or an average slope $m \equiv \langle \nabla h \rangle$ within an interval of length l of the interface, the result Eq. (3.9b) means that the velocity of the interface within that interval is approximately given by

$$v(m) \approx c + \frac{\lambda}{2} m^2. \tag{3.10}$$

This $v(m)$ is thus the slope-dependent velocity which should be observed in the coarse-grained scale l. One should find a parabolic dependence which, when fitted by Eq. (3.10), gives an estimate for the coefficient of the nonlinear term, λ [26, 9].

From experimental data the slope-dependent interface velocity can be evaluated by applying, *e.g.*, the procedure described by Albert *et al.* [1]: the discretised interface $h_i(t)$ of length N $(= L/\Delta x)$ is partitioned into overlapping segments of length l. The local slope $s_i(t)$ of each segment i at time t is determined by a linear fit to the interval $(i, i + l - 1)$, with $i = 1, 2, \ldots, (N - l + 1)$. The same partitioning and linear fits are then repeated for the interface at time $t + \tau$, and the average (local)

velocity of each segment is determined from

$$u_i(t) = \frac{1}{l}\sum_{j=0}^{l-1}\left[\frac{h_{i+j}(t+\tau) - h_{i+j}(t)}{\tau}\right] . \tag{3.11}$$

The average velocity of all segments with average slope s (averaged over the initial (at time t) and 'final' slope (at time $t+\tau$)), is then given by

$$u(s) = \frac{1}{N(s)}\sum_{i,t} u_i(t) , \tag{3.12}$$

where $s_i(t) \in]s - \Delta s/2, s + \Delta s/2]$ with Δs a suitable discretisation length for slopes, and $N(s)$ is the number of such segments. If this $u(s)$ plotted as a function of s indeed has a parabolic form, it indicates that a slope-dependent nonlinear term is present in the growth equation.

3.4.2 D/ν from the equal time correlation functions

Since for one-dimensional interfaces stationary height fluctuations are independent of the nonlinear term in Eq. (3.5), all stationary, equal-time correlation functions can be easily computed. The stationary distribution is Gaussian, with variance [40]

$$\lim_{t\to\infty} \langle |\, \hat{h}(k,t)|^{\,2} \rangle = \frac{D}{\nu L k^2} \tag{3.13}$$

for the discrete Fourier modes (see Eqs. (3.25) and (3.22) below). Consequently, the amplitude of the spatial correlation function in Eq. (3.15), for large r, is given by $A = D/\nu$.

3.4.3 Universal (dimensionless) quantities

In a typical dynamic renormalization group (DRG) analysis, one obtains a RG flow for a dimensionless coupling constant, which provides a measure of the effective nonlinearity present in the system. For the KPZ equation, this coupling constant is [35,26]

$$g(b) = \left(\frac{\lambda^2(b)\, D(b)}{\nu^3(b)}\right)^{1/2} b^{(2-d)/2} , \tag{3.14}$$

where b is the scale of coarse graining, and $\lambda(b)$, $D(b)$, and $\nu(b)$ are renormalised parameters. The scaling exponents are then evaluated at the fixed point of the RG flow, $g^* = g(b \to \infty)$. Hwa and Frey [32] showed that g^* plays the role of a crossover scale between the correlation function's space-dependent and time-dependent regimes,

and may also be expressed in terms of a *universal ratio* of amplitudes A and B,

$$G_2(r) = A\, r^{2\chi}; \quad C_2(t) = B\, t^{2\beta}\,, \tag{3.15}$$

such that

$$g^* = \frac{\lambda}{2}\left(\frac{A}{B^{z/2}}\right)^{1/\chi}\,. \tag{3.16}$$

They solved the dimensionless form of the universal scaling function, which the correlation function obeys, for an arbitrary substrate dimension d, and explicitly for $d = 1$ using mode-coupling theory. The value predicted by them for the universal coupling constant is $g^* \simeq 0.87$.

Using a scaling approach, Amar and Family derived an expression for the correlation function amplitudes as a function of macroscopic parameters of the KPZ equation [3]:

$$R_G = \frac{B}{|\lambda|^{2\beta} A^{\beta+1}}\,, \tag{3.17}$$

where A and B are determined in Eq. (3.15) above. For the KPZ equation in $1+1$ dimensions, from simulations of its three different discrete realisations and from a mode-coupling calculation, they determined the correlation function amplitudes $R_G \simeq 0.71$ ($g^* \simeq 0.834$) and $R_G \simeq 0.63$ ($g^* \simeq 0.999$), respectively. It is also possible to derive an expression for the behaviour of the asymptotic surface width amplitudes [2,3]:

$$R = \frac{C_t}{|\lambda|^{\beta} C_L^{\beta+1}}\,; \quad C_t = w(\infty, t)/t^{\beta} \text{ and } C_L = w(L, \infty)/L^{\chi}\,. \tag{3.18}$$

The amplitude ratio R has not been determined for our experiments due to difficulties in obtaining accurate values for the interface width $w(t)$.

3.5 KPZ model parameters II

In this section two methods used to identify at the same time all the parameters of the evolution equation are summarised. The methods for the extraction of the scaling behaviour from experimental data using the correlation functions were already covered in Chapter 2. With these two methods, it would in principle be possible to determine also the form of the effective evolution equation, but practical difficulties related *e.g.* to discreteness and statistics effects prevent them from adequately treating terms that include higher-order derivatives. Their use thus appears to be limited to the leading terms only, *i.e.*, to equations like the KPZ equation.

3.5.1 Inverse method

The inverse method applied here closely follows the general approach proposed by Lam and Sander [41]: the evolution equation for the fronts is first written in the form

$$\frac{\partial h(x,t)}{\partial t} = \mathbf{a}\cdot\mathbf{H}(x,t) + \eta(x,t), \tag{3.19}$$

where $\mathbf{a}$ is a vector containing the relevant coefficients of the equation, *e.g.* $\mathbf{a} = (\nu, \lambda/2, \dots)$, and $\mathbf{H}(x,t)$ is a vector containing derivatives of $h(x,t)$ and powers of these derivatives. Since the observed quantities are determined from the experimental data that are composed of digital front images, the single-valued function $h(x,t)$ is replaced by $h_i(t)$ with subscript i the lattice index. The lattice has spacing Δx and $N \equiv L/\Delta x$ sites, where L is the sample width. The time interval between consecutive images is denoted by Δt. One then discretises Eq. (3.5) so that it is coarse grained up to length l and up to time τ (a multiple of Δt), such that

$$\frac{\Delta h_i(t)}{\tau} \simeq \mathbf{a}\cdot\mathbf{H}_i(t) + \eta_i(t)\ . \tag{3.20}$$

For the KPZ equation, Eq. (3.5), the parameter vector $\mathbf{a}$ and the interface derivative vector $\mathbf{H}$, respectively, are of the form

$$\mathbf{a} = \left[c, \nu, \frac{\lambda}{2}\right] \quad \text{and} \quad \mathbf{H}_i(t) = \left[1, \nabla^2 h, (\nabla h)^2\right]. \tag{3.21}$$

Since the average height of the fronts $\overline{h}(t) = (1/N)\sum_i h_i(t)$ had in all cases a clear linear trend in time, the zero-slope velocity c was assumed to be constant. To determine $\mathbf{H}_i(t)$, all the fronts are first coarse grained by truncating their Fourier components with wavelengths smaller than l. This means that from the (discrete) Fourier transforms of the front heights,

$$\hat{h}_{q_n}(t) = \int_{-L/2}^{L/2} dx\, h(x,t)\, e^{-i\,q_n x}\ , \tag{3.22}$$

all wavelength components $\hat{h}_{q_n}(t)$ with a wavenumber $q \geq \pi/l$ are set to zero. For $\Delta h_i(t)/\tau$ we used the forward difference approximation with $\Delta h_i(t) = h_i(t+\tau) - h_i(t)$. Subsequent differentiations and multiplications were carried out in the Fourier and the real spaces, respectively. The parameter vector $\mathbf{a}$ was then determined by solving $\min_{\mathbf{a}} \mathcal{J}(\mathbf{a})$, where

$$\mathcal{J}(\mathbf{a}) = \left\langle \left[\frac{\Delta h_i(t)}{\tau} - \mathbf{a}\cdot\mathbf{H}_i(t)\right]^2 \right\rangle_{i,t}. \tag{3.23}$$

Notice that in Eq. (3.23) it is implicitly assumed that the noise characteristics are the same for all experimental data. Moreover, basically one should also include in Eq. (3.23) the restriction of relevant coefficients into physically reasonable values (*e.g.*, c and ν should be positive). Here, the relevance is checked only afterwards. Once a minimiser $\mathbf{a}^*$ of Eq. (3.23) is determined, the noise correlator D follows from

$$D = \frac{l\tau}{2}\,\mathcal{J}(\mathbf{a})\;. \tag{3.24}$$

All the parameters c, ν, λ, and D thus obtained depend on both the spatial and the temporal resolution l and τ, respectively. For c and λ convergence to constant values independent of coarse graining should however appear, while such convergence is not expected for ν nor D.

3.5.2 Pseudo-spectral method

Giacometti and Rossi [20] have proposed a method for extracting the coupling parameters of the KPZ equation from experimental snapshots of successive interface profiles. This method hinges on two main ingredients. First, a pseudo-spectral scheme is used to simulate the KPZ equation, and this scheme can be considered as an improved discretisation in comparison with the standard real-space finite-difference ones. Using

$$h(x,t) = \frac{1}{L}\sum_{n=-\infty}^{+\infty} \hat{h}_{q_n}(t) e^{iq_n\,x}\;, \tag{3.25}$$

where the Fourier components are associated with wave numbers $q_n = 2\pi n/L$, in Eq. (3.5), an infinite system of coupled Langevin equation is obtained:

$$\begin{aligned}\frac{d\hat{h}_{q_n}(t)}{dt} &= cL\delta_{n,0} - \nu q_n^2 \hat{h}_{q_n}(t) + \\ &\quad -\frac{\lambda}{2L}\sum_{m,m'=-\infty}^{\infty} q_m q_{m'} \hat{h}_{q_m}(t)\hat{h}_{q_{m'}}(t)\delta_{n,m+m'} + \hat{\eta}_{q_n}(t)\;.\end{aligned} \tag{3.26}$$

The spectral approximation now amounts to projecting the above infinite system on the space of periodic functions of period L with a finite number of Fourier modes $\hat{h}_{q_n}$ ($|q_n| \le q_{N/2}$). All equations retain their original form with the proviso that the infinite sums $\sum_{n=-\infty}^{\infty}$ are now replaced by finite ones $\sum_{n=-N/2}^{N/2}$. This procedure thus assumes that $\hat{h}_{q_n} = 0$ for any $n > N/2$, and the original continuum equation is reduced to a set of $N+1$ real Langevin equations. As a matter of fact, this preserves both the correct steady state distribution and the coarse-graining properties of the corresponding continuum equation.

Second, the reconstruction algorithm is based on the time evolution of correlation functions. The evolution equations for correlation functions follow from

Eq. (3.26) and can be written in the form

$$\frac{d}{dt}g_2(t) = -2\nu g_4(t) + 2DQ_2 \quad \text{and} \quad \frac{d}{dt}g_0(t) = cL + \frac{\lambda}{2}g_2(t) \tag{3.27}$$

where $g_0(t) \equiv \langle \hat{h}_{q_0}(t) \rangle$, $g_{2p}(t) \equiv L^{-1} \sum_{n=-N/2}^{N/2} q_n^{2p} \langle |\hat{h}_{q_n}(t)|^2 \rangle$ for $p = 1, 2, \ldots$, and $Q_2 = \sum_{-N/2}^{N/2} q_n^2$. These functions do satisfy a deterministic evolution equation, which allows the use of standard least-squares procedures to identify the coupling parameters.

For a given realisation, the experimental interface is observed at times $t_k = k\Delta t$; $k = 1, 2, \ldots, pM$, where Δt is the measurement sampling time. By integrating Eqs. (3.27) during p sampling times Δt, one obtains

$$\frac{g_2(T_{k+1}) - g_2(T_k)}{T_{k+1} - T_k} = -2\nu \frac{1}{T_{k+1} - T_k} \int_{T_k}^{T_{k+1}} g_4(t)\, dt + 2DQ_2 \,, \tag{3.28}$$

where time $T_k = kp\Delta t$ $(k = 1, \ldots, M)$, and

$$\frac{g_0(T_{k+1}) - g_0(T_k)}{T_{k+1} - T_k} = cL + \frac{\lambda}{2} \frac{1}{T_{k+1} - T_k} \int_{T_k}^{T_{k+1}} g_2(t)\, dt \,. \tag{3.29}$$

If Δt is smaller than the characteristic time of the dynamics, one may approximate the time integrals in Eqs. (3.28) and (3.29) as averages over the p intermediate sampling times, thereby obtaining $M - 1$ linear constrains on the parameters ν, D and c, λ. A simple least-squares calculation then determines ν and D from Eq. (3.28), and c and λ from Eq. (3.29).

Chapter 4

Experiments and Data

A convenient approach to study kinetic roughening experimentally is to analyse the propagation of slow-combustion fronts in paper sheets. An early attempt was made by Zhang *et al.* [74], whose experiments were very helpful for the design and construction of our own experimental set up. Experiments on flame fronts in paper were later carried out by Balankin and Matamoros [7]. However, this latter experiment was a 'post-mortem' study, *i.e.*, the flame fronts were quenched after they reached the middle line of the sheet, and the quenched fronts were scanned. Both these studies reported estimates only for the roughness exponent χ.

Our experiments were conducted under controlled conditions inside a combustion chamber, where the air flow and the angle between it and the paper sheets were adjustable. The paper sheets were ignited from one end using a heating wire, and the time evolution of the combustion front was recorded using a three-CCD-camera system connected to a computer. The time-coded digital images of the combustion fronts were then post-processed to map the position of the *front line* with a discrete single-valued function. The experimental arrangement and the camera set up are shown in Figure 4.1.

The post-processing of the digital gray-scale images from the three cameras included compression of the individual frames, determination of the front position in each of them, correction of the cylindrical distortions, and joining of the three height functions thus determined. In more detail this process can be divided into four separate steps.

1. The frames were compressed by recording a narrow stripe around the front line. Since the images were taken in darkness, the only visible object was the combustion front.

2. The front height position in each frame was determined by finding the pixels brighter than a given gray-scale value. A single-valued front line was fitted into the brightness profile. In the intervals, where a front line could not be identified, an interpolating straight line was fitted.

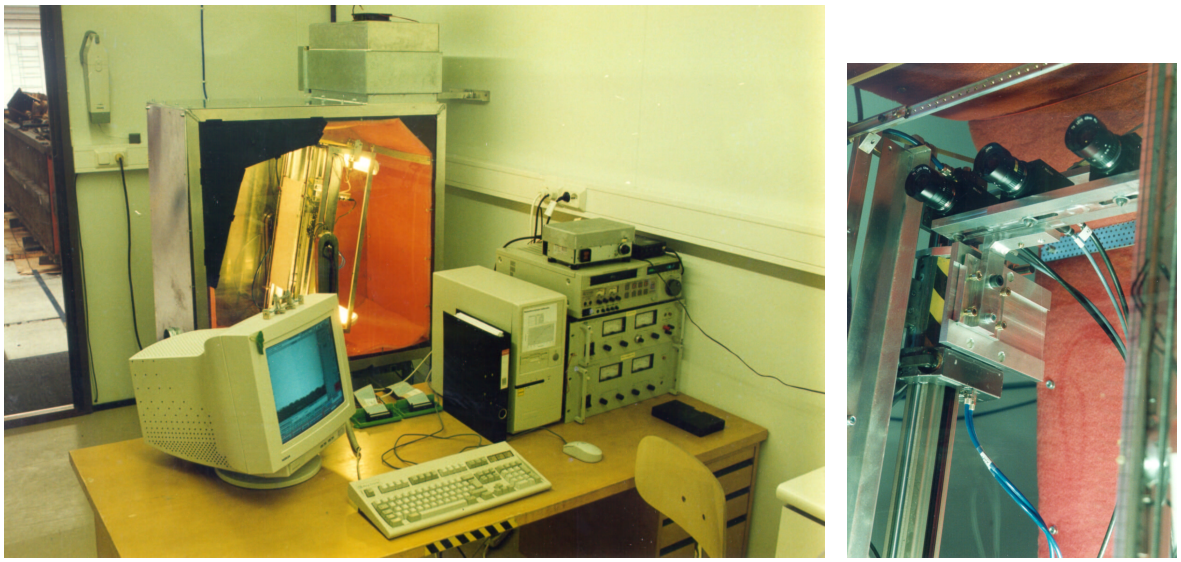

FIGURE 4.1 The experimental arrangement (left) incorporated a combustion chamber, with an adjustable paper holder and a three-CCD-camera setup (right) that was connected to a computer with necessary hardware and software for recording and processing digital images.

3. The cylindrical image distortions caused by the lenses were corrected using nonlinear warping. The method needs a collection of two-dimensional landmark points whose true locations are known together with their distorted images. These were then used to define a global warping function, that was used to correct the position data of the individual cameras before joining them.

4. Since the camera system was moved in regular intervals along the direction of propagation, and the front height $h(x,t)$ was given as the perpendicular distance from the lower edge of the image, the actual value of the front height had to be estimated by first determining the average front height $\overline{h}(t) \equiv \langle h(x,t) \rangle_x$ and then fitting straight lines into the $(t, \overline{h}(t))$ data between camera moves. These fitted lines were then used to extrapolate the position of the lower edge of the image after the camera moves.

An example of a mapped position of a front line from lens-paper burns, and individual images it was reconstructed from, is displayed in Figure 4.2.

Experiments were done on sample sheets of mainly three different paper grades. In order to study the effects of the properties of the random medium on front propagation, the sample sheets were chosen with varying basis weight, *i.e.*, 70 and $80\,\mathrm{g/m^2}$ for the two copier-paper grades, and $9.1\,\mathrm{g/m^2}$ for the lens-paper grade, respectively. Tests were also done on samples of cigarette paper that is anisotropic and contains nontrivial correlations, and is therefore less than optimal for studies of propagating interfaces in random medium. Despite this fact, the results for cigarette paper [50] were consistent with those for the copier papers.

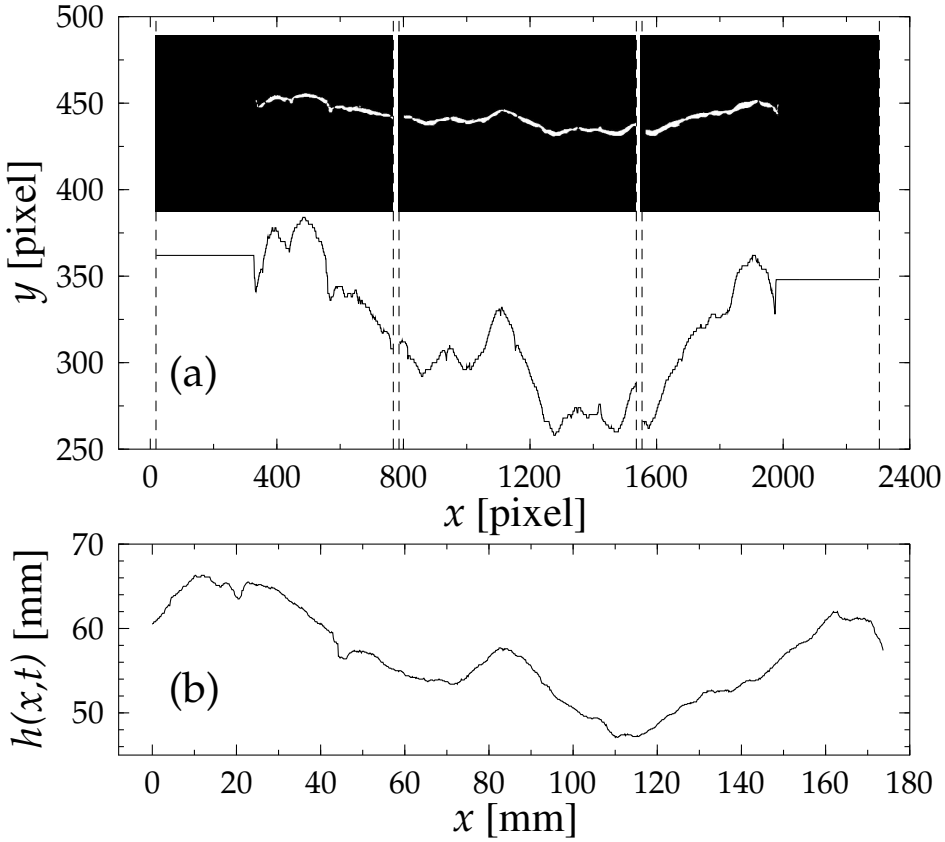

FIGURE 4.2 (a) The mapped position of the front line from a lens-paper burn. The edges of the recorded images are shown by the vertical dashed lines. The insets show the individual images recorded from the three CCD-cameras. (b) The single-valued front-height function $h(x,t)$ after the cylindrical image distortions were corrected and the data were joined together.

To guarantee flameless burning (smouldering fronts) and a continuous front line, the sheets were treated with a potassium nitrate (KNO_3) solution. A detailed description of the experimental arrangements, the samples, and sample preparation, can be found in Refs. [50, 57] and in the PhD Thesis by Markko Myllys [56].

Our results were obtained by analysing those burns in which the front did not get pinned and the accidental defects in the observed data were few. By accidental defects we mean digitising errors and sharp natural defects caused *e.g.* by ash masking the front position. Such burns, where the front was clearly lagging behind on the edges of the sheet, were in some cases also discarded. In most cases, this last effect was restricted to within a few centimetres along the edges of the sheet, so we just omitted these strips from the analyses. Therefore, the system sizes were approximately 28 and $14\,\mathrm{cm}$ for the copier-paper and the lens-paper burns, respectively. The volume of the combustion chamber limited the maximum size of the sample sheets to $400 \times 600\,\mathrm{mm}$. The smaller system size in the case of lens paper was also due to the

higher velocity of the fronts, which led to a shorter period of saturated behaviour at the end of the burns than in the case of copier-paper samples of similar width.

The limited size of the samples had to be taken into account when we wanted to analyse the scaling behaviour of the smouldering fronts in the saturated regime. If the ignited front was very straight (in fact technically quite difficult to achieve), the evolving front reached the saturated regime only at the last stages of the burn, and its scaling behaviour could not be analysed with high enough accuracy. This problem was bypassed by having a somewhat uneven ignition so that an initial roughness was created in the fronts. In this way a much longer saturated regime was achieved. The possible effects of initial roughness were later studied by simulations of a discretised KPZ equation, and the scaling properties in the saturated regime of the evolving fronts were found to be independent of initial roughness. The initial roughness of the fronts was however a reason to analyse their dynamic scaling from the temporal height-height correlation functions rather than from the interface widths. Finite-size scaling of local width could however be used in addition to correlation functions.

It proved to be of crucial importance to do extensive averaging over independent slow-combustion fronts. In all samples there was quenched noise due to density variations typical of paper-like materials, and the noise affecting the fronts also included dynamical effects, such that there were wide fluctuations in individual fronts, also from burn to burn. Dynamical fluctuations can be related to fluctuating flow of air created by a burning front, and this flow will give rise to fluctuations in the 'effective' heat conductivity (due to convective transfer of heat) and in cooling. We found that averaging over approximately ten independent burns is needed for fairly reliable estimates for the quantities measured. For copier burns this means in practice averaging over up to about 40 000 individual fronts, and for lens paper, with much faster propagating fronts, over several thousand individual fronts. For the lens paper, averaging was hampered by the shortness of the saturated regime.

The averaging of the data was done by first calculating for each burn separately the mean value of the quantity to be averaged. The average value for the set of burns was then calculated as a weighted average of these mean values such that the weight of a burn is the fraction of fronts in that burn from the total number of fronts in the set.

Chapter 5

Filtering of Erratic Noise

In this chapter we briefly describe the new filtering method used to reduce digitising errors and other erratic factors in the recorded fronts. For digital images containing noise and other degradations due to non-Gaussian distributions and outliers, so-called robust methods must be applied for proper restoration (see *e.g.*, [31, 65] and references therein). The basic principle behind such methodology is simple: whereas the discrete, univariate sample mean $\min_{\mu_2} \sum_{i=1}^{N} |\mu_2 - x_i|^2$, *i.e.* $\sum_{i=1}^{N} (\mu_2^* - x_i) = 0$, is sensitive to the actual distance between the estimator and the given data, the corresponding median $\min_{\mu_1} \sum_{i=1}^{N} |\mu_1 - x_i|$, i.e. $\sum_{i=1}^{N} \operatorname{sign}(\mu_1^* - x_i) = 0$, is not. Here the variables marked with an asterisk are solutions of the respective minimisation problems.

The most commonly used robust image restoration method is the so-called median filter which uses an a priori chosen or an adaptively determined window for locating the seek of the median value [23]. Although this procedure is robust for single outliers, the median filter does not contain any control of smoothness of the restored image. This is why the obtained result has a staircase- or rump-like structure for small windows, becomes more and more blurred when the window size increases.

Next we describe the main ideas of the restoration scheme in a continuous setting. The restored image $u(x,t)$ is obtained as the solution of the optimisation problem

$$\min_u \mathcal{J}(u) \;\text{ for }\; \mathcal{J}(u) = \int_\Omega \left[|u - z| + \frac{\beta_1}{2} \left| \frac{\partial u}{\partial x} \right|^2 + \frac{\beta_2}{2} \left| \frac{\partial u}{\partial t} \right|^2 \right] dx\, dt\,, \tag{5.1}$$

where z represents the experimental data. The cost functional to be minimised in Eq. (5.1) consists of two parts, where the first part introduces a robust and outlier-insensitive fitting between the solution and the noisy observation in the L^1-norm. The second part controls the regularity of the solution in an orthotropic manner allowing one to impose different kinds of behaviour in the x and t directions. For $\beta_1, \beta_2 > 0$, $\mathcal{J}(u)$ is strictly convex, so that Eq. (5.1) admits a unique solution u^*

[17]. However, due to the L^1-term, $\mathcal{J}(u)$ is non-differentiable in the classical sense (derivative of function $|x|$ at zero is multi valued) so that ordinary optimisation methods like the steepest descents or conjugate gradient method, cannot be applied for solving Eq. (5.1) [48, 60].

The actual discrete counterpart of Eq. (5.1) is given by

$$\min_{u\in\mathbb{R}^N} J(u) \text{ for } J(u) = |M(u-z)|_1 + \frac{\beta_1}{2}u^T K_x\, u + \frac{\beta_2}{2}u^T K_y\, u. \tag{5.2}$$

Here, $|v|_1 = \sum_i |v_i|$ denotes the discrete l_1-norm, v^T the transpose of a vector v, K_x, K_y directional stiffness matrices and M the diagonal, lumped mass matrix of FEM discretization of Eq. (5.1) [37]. The heuristic interpretation of Eq. (5.2) is the following. Locally a median-like value is restored and global smoothness is assured by the orthotropic regularization that defines a norm which is equivalent to a (discrete) H^1-norm. Both the shape of the local neighbourhood and the strongness of fitting are determined by the chosen values of β_1 and β_2.

In practice, we first apply a technique similar to that of Eq. (5.2) on the one-dimensional boundary of the experimental data. These presmoothed values are then used as a non-homogeneous boundary condition in Eq. (5.2). The algorithm used in this work can be found in the Appendix of Ref. [51] and a more detailed discussion in Ref. [22]. One example of the effect of filtering on the data is shown in Figure 5.1.

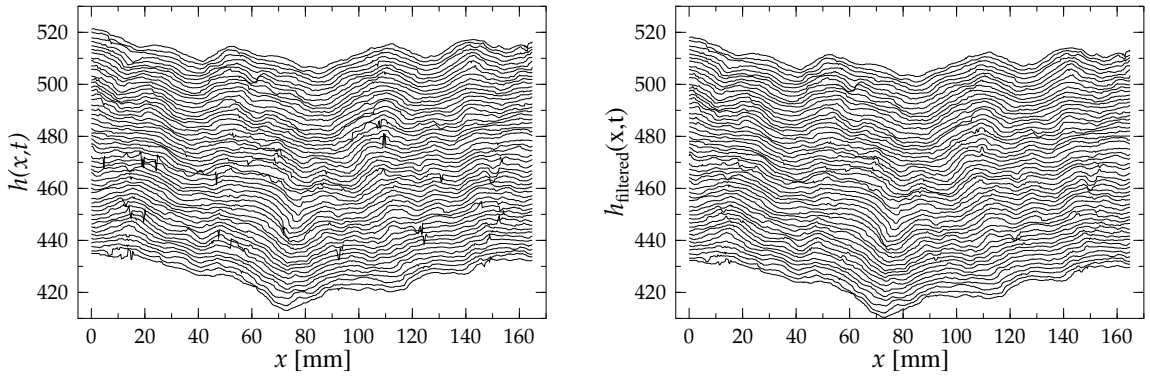

FIGURE 5.1 The original ($h(x,t)$) and filtered ($h_{\text{filtered}}(x,t)$) front-height data for a lens-paper burn. In filtering $\beta_1 = \beta_2 = 0.01$ were used.

Chapter 6

Results and Discussion

6.1 Scaling of correlation functions and front width

The evolution and the scaling behaviour of the fluctuating slow-combustion fronts were monitored by measuring first of all the height-height correlation functions (HHCF) and the local width (LW) (see Chapter 2). The results of the observed scaling behaviour are given here for the two grades of copier paper, and a grade of lens paper.

6.1.1 Crossover behaviour

The height-height correlation functions and local front width all show a crossover from a short-scale to an asymptotic behaviour which prevails at large temporal and spatial scales. Such a crossover is observed for all paper grades (Figures 2.1). The related crossover scale was for the spatial behaviour $r_c = 4.7 - 11\,\mathrm{mm}$, and for the temporal behaviour $t_c = 3.7 - 27\,\mathrm{s}$ (see Table I in Ref. [57]). The crossover scales r_c and t_c provide an extra time and an extra length scale, respectively, in addition to the sample width, and the correlation length and the related time scale. These additional scales should be taken into account when analysing the scaling properties of moving fronts. In the usual scaling hypothesis one assumes that the sample width and the correlation length are the only relevant length scales in the system (Chapter 2). The crossover values given above [57] were determined as the crossing points of power laws fitted separately to the short-range (SR) and long-range (LR) parts of the curves.

This crossover phenomenon was first observed [30] in fluid-flow experiments, and very recently also [69] in magnetic flux fronts penetrating in a high-T_c thin-film superconductor. Several possible mechanisms have been suggested for this phenomenon, *i.e.*, quenched [70,42,43] or power-law correlated [54,8] or power-law distributed [75] noise or directed percolation depinning (DPD) [6,5,4] (see also Ref. [26] for a review). Before the present work, the reasons for the crossover behaviour were

not cleared up, although power-law distributed amplitudes in the effective noise were reported in Ref. [29].

It appears that the SR correlations in the effective noise, either quenched or annealed or both, are likely to be responsible for the crossovers and the related higher apparent exponents at short range, see below. Also, at least in the present case, the effective noise clearly is partly of dynamical origin as mentioned in Chapter 4. This becomes evident from the fact that the temporal crossover scales are always longer than the related spatial crossover scales along the fronts divided by the average front velocities.

For a more detailed analysis of this noise, including simulation results for a discrete KPZ equation with real (mass distributions measured on paper samples) and randomised noise, we refer to the Ph.D. Thesis by Markko Myllys [56].

6.1.2 Kardar-Parisi-Zhang scaling

The long-range (asymptotic) behaviour is similar in all paper grades. In the log-log scale the correlations functions, *e.g.*, display asymptotically linear behaviours with slopes independent of the grade of paper. The possible scaling can be most reliably resolved by analysing the running values of the effective exponents for the height-height correlation functions, χ_{eff} as defined in Eq. (2.6), and similarly for β_{eff}.

It is evident from Figure 6.1 that the running effective exponents asymptotically have clear plateaux with values $\chi_{\text{eff}} \simeq 1/2$ and $\beta_{\text{eff}} \simeq 1/3$. This proves that, beyond the crossover scales, the dynamics of slow-combustion fronts in paper belong to the KPZ universality class (with uncorrelated white noise). For a more accurate determination of the scaling exponents one can now analyse in different ways the asymptotic regimes of the correlation functions and also the interface width.

The scaling exponents shown in Table 6.1 were determined by performing linear least-squares fits to the corresponding height-height correlation functions [Eq. (2.3)] in the LR scaling regime. An independent estimate for the roughness exponent χ was obtained by fitting the appropriate power law in the LR local width data. The early-time behaviour of the front width also gave an estimate for the growth exponent β. As noted in Chapter 2, a more accurate determination of the scaling exponents necessitates the removal of the 'intrinsic' widths from the correlation functions and local front widths. The values obtained in this way are denoted by asterisks in the "Method" column of Table 6.1. The most reliable results in Table 6.1 (6.2) were obtained using the height-height correlation function and the local width [57], and they were averages over 10-11 burns of the $70\,\mathrm{g/m^2}$ and 6-18 burns of the $80\,\mathrm{g/m^2}$ copier paper, and 24-32 burns of the $9.1\,\mathrm{g/m^2}$ lens paper.

The largest deviations are displayed by the lens paper as in this case the saturated regime was too short for an accurate determination of β. Also the poor time resolution in the $70\,\mathrm{g/m^2}$ copier papers case, affected the temporal scaling but mainly in the SR regime (see below). Because of experimental limitations and the relative

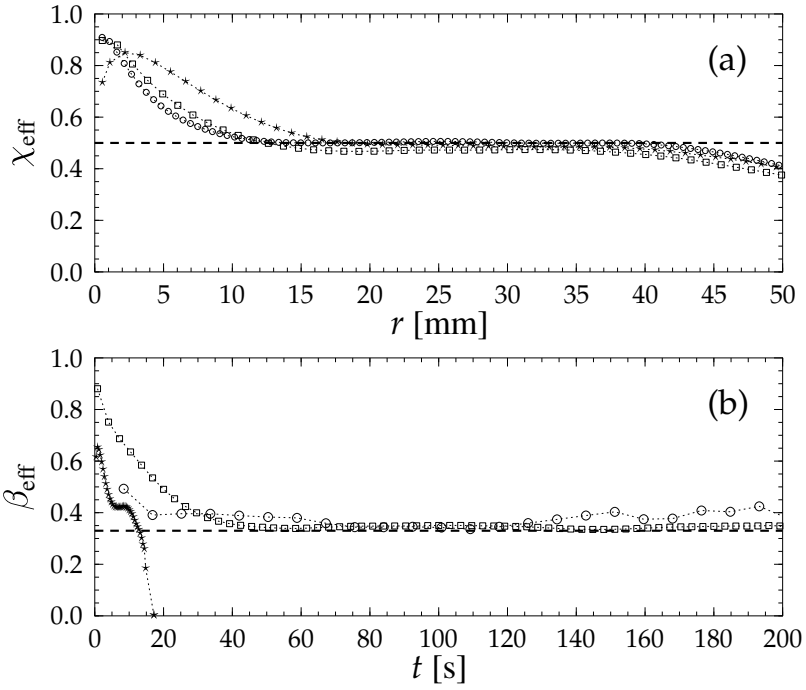

FIGURE 6.1 The running exponents (a) $\chi_{\rm eff}(r)$ and (b) $\beta_{\rm eff}(t)$ calculated for three paper grades from the height-height correlation functions $G_2(r)$ and $C_2(t)$ (Figure 2.1), respectively, after the intrinsic widths were subtracted. The results were averages over 10 of the 70 $\mathrm{g/m^2}$ (○) and 6 of the 80 $\mathrm{g/m^2}$ (□) copier paper burns, and 32 of the 9.1 $\mathrm{g/m^2}$ lens paper burns (★). The dashed lines in the above figures denote (a) $\chi_{\rm eff} \simeq 1/2$ and (b) $\beta_{\rm eff} \simeq 1/3$, respectively.

TABLE 6.1 Scaling exponents for the Kardar-Parisi-Zhang-like scaling in slow combustion of paper. ($^{(*)}$Estimates were obtained after an intrinsic width was subtracted from the correlation function or the local front width.)

Scaling exponent	Paper grade			Method	Reference
	70 $\mathrm{g/m^2}$	80 $\mathrm{g/m^2}$	9.1 $\mathrm{g/m^2}$		
β_{LR}	–	0.32(1)	–	HHCF	[50]
	0.40(3)	0.39(3)	0.46(2)	HHCF	[57]
	0.29(3)	0.32(3)	0.28(5)	LW	[57]
	0.36(3)	0.34(4)	0.43(6)	HHCF$^{(*)}$	[57]
χ_{LR}	–	0.48(1)	–	HHCF	[50]
	0.53(3)	0.51(3)	0.53(4)	HHCF	[57]
	0.57(1)	0.55(2)	0.56(2)	LW	[57]
	0.50(4)	0.47(4)	0.50(6)	HHCF$^{(*)}$	[57]
	0.56(1)	0.52(5)	0.51(1)	LW$^{(*)}$	[57]

sizes of the crossover scales, the range in which we were able to observe the (asymptotic) scaling was somewhat limited. It is not realistic to significantly increase the width of the paper samples so as to extend the scaling regime by *e.g.* an order of magnitude. In the case of the structure factor $S(k)$ (Figure 6.2) doubling the system size would increase the points in the asymptotic region only by one. The only way to achieve a notable increase in the size of the scaling regime would thus be to find a material with much smaller crossover scales. Obviously we can also support the conclusions by analysing the scaling behaviour through other quantities in addition to the mere scaling exponents.

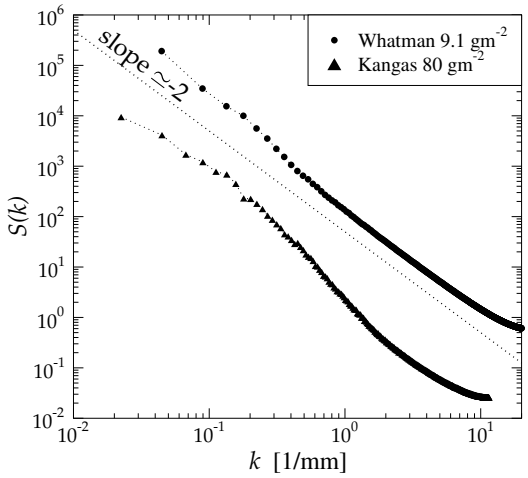

FIGURE 6.2 The structure factor $S(k)$ determined for slow-combustion fronts in $9.1\,\mathrm{g/m^2}$ lens paper and $80\,\mathrm{g/m^2}$ copier paper. The dotted line corresponds to the asymptotic KPZ value $\chi = 1/2$ via $S(k) \sim k^{-2\chi-1}$.

As already noted above, both the growth and the roughening exponent were determined and found consistent with those of the KPZ equation with uncorrelated white noise. Previous experiments had mostly obtained values for only the roughness exponent χ (see, *e.g.*, Refs. [66, 30, 72, 33]), and these values exceeded the KPZ result $\chi = 1/2$. The only exceptions to this general trend were Refs. [33, 30], where values consistent with that of the KPZ equation were reported. First indications that the slow-combustion fronts in paper follow the KPZ scaling at large enough time and length scales were reported in Ref. [50]. We expect that the higher values reported for the scaling exponents can be related to the short-range behaviours in the systems analysed, before the asymptotic KPZ behaviour sets in, as these values are similar to the SR apparent exponents found in the present case, and are caused by system specific noise. Also it was crucial to do extensive averaging over independent slow combustion fronts. There is also theoretical indication [63, 64] that slow-combustion fronts should asymptotically display KPZ dynamics.

6.1.3 Anomalous scaling

The running effective exponents in Figure 6.1 also show that there appears to be no true scaling below the crossover scales, *i.e.*, the running exponents do not show plateaux there, given the resolution of the experimental setup. The estimates for the apparent exponents in the SR regimes, shown in Table 6.2, were calculated by performing linear least-squares fits to the corresponding height-height correlation functions, Eq. (2.3), and the local width, Eq. (2.12). The methods used in these fits were the same as the ones used for the asymptotic scaling in Section 6.1.2, including the removal of additive constant factors in the correlation functions and the local front widths.

The results in Table 6.2 show that in the SR regime below the crossover length, the spatial height-height correlation function appears to scale with a rather large effective exponent $\chi_{SR} \simeq 0.9$ for the copier paper grades, and 0.85 for the lens paper. The temporal correlation functions with the intrinsic width removed were analysed in the SR regime only for the heavier copier paper and the lens paper due to the poor time resolution ($\Delta t = 4.2\,\mathrm{s}$) in the $70\,\mathrm{g/m^2}$ paper data. The short-time growth exponent β_{SR} was, again, rather large, $\beta_{SR} = 0.75(5)$ and $0.64(3)$ for the $80\,\mathrm{g/m^2}$ copier paper and $9.1\,\mathrm{g/m^2}$ lens paper, respectively. In either cases, our measured SR exponents did not agree with the expectation $\beta \simeq \chi \simeq 0.75$ based on the DPD model [42, 6].

TABLE 6.2 The apparent scaling exponents at short time and length scales. ($^{(*)}$Estimates were obtained after an intrinsic width was subtracted from the correlation function or the local front width.)

Scaling exponent	Paper grade			Method	Reference
	$70\,\mathrm{g/m^2}$	$80\,\mathrm{g/m^2}$	$9.1\,\mathrm{g/m^2}$		
β_{SR}	0.59(4)	0.69(2)	0.61(2)	HHCF	[57]
	-	0.75(5)	0.64(3)	HHCF$^{(*)}$	[57]
χ_{SR}	0.88(2)	0.89(2)	0.83(1)	HHCF	[57]
	0.81(6)	0.83(5)	0.81(1)	LW	[57]
	0.90(3)	0.90(4)	0.85(1)	HHCF$^{(*)}$	[57]
	0.84(6)	0.87(8)	0.95(6)	LW$^{(*)}$	[57]

Higher-order correlation functions, Eq. (2.3), were also determined to check the possible multiscaling properties of the slow-combustion fronts [58, 57]. The behaviour of these higher-order correlation functions indicates that, in the asymptotic KPZ regime, the interfaces are simply self-affine. On the other hand, in the SR regime, the slopes of the spatial and temporal correlation functions depend on

the order q of the correlation function, *i.e.*, they show *apparent multiscaling* [11,10,8]. As there is no SR scaling regime (as deduced from the running exponents), there is no true self affinity nor multiscaling. This agrees qualitatively with the numerical study [42] of Leschhorn in which he showed that the moving interfaces described by the quenched KPZ equation for F slightly larger than F_c are not self-affine. However, while in Ref. [42] the effective growth and roughness exponents at very short time and length scales were roughly independent of q, in our case they display a strong q dependence. The possible reasons for this are discussed in Section 6.2 below.

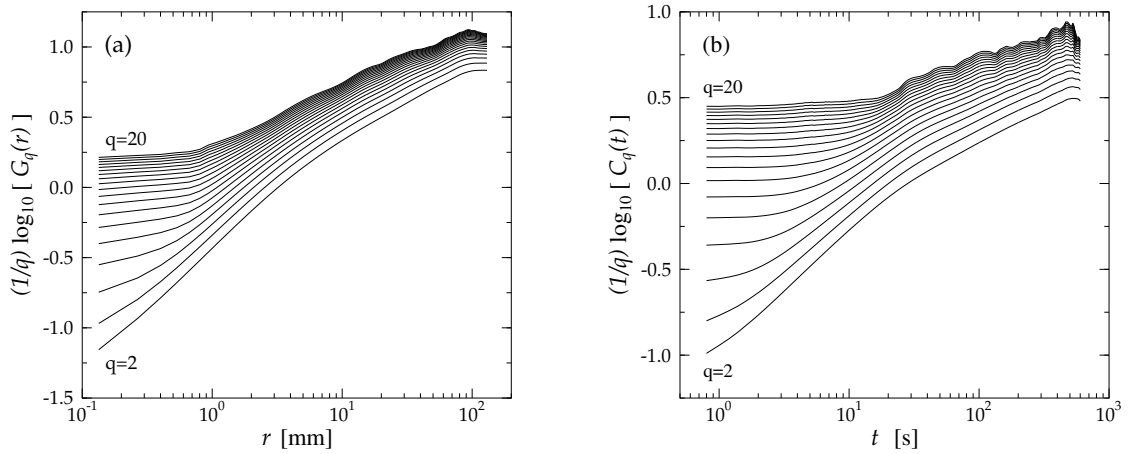

FIGURE 6.3 The (a) spatial and (b) temporal qth order correlation functions $G_q(r)$ and $C_q(t)$ averaged over 10 burns for the $70\,\mathrm{g/m^2}$ copier paper and 20 burns for the $80\,\mathrm{g/m^2}$ copier paper, respectively.

Concerning the origin of the apparent multiscaling, it is evident that regions with high gradient (in absolute value) are amplified in the higher-order correlation functions. Distinct regions of such high gradient values are evident if successive fronts are plotted as surface diagrams (see Figure 5.1). Digitising errors and sharp natural defects in the observed data also make a contribution to the apparent multiscaling properties, and should be filtered out as artifacts. Also some SR effects due to asymptotically irrelevant terms in the evolution equation could not be ruled out based on our simulation results [56] and the results given by the inverse methods (see below).

6.2 Scaling and noise

Since various experiments on kinetic roughening have mostly failed to demonstrate the KPZ scaling, it has been suggested that this could result from nontrivial effective noise: Medina, Hwa, and Kardar [54] carried out simulations for spatially and

temporally correlated Gaussian noise, and Zhang [75] introduced a power-law distribution for noise amplitudes. It was also proposed that the observed scaling could be understood in terms of the DPD model [6, 4]. As noise is also expected to be relevant for the short-range behaviour of slow-combustion fronts, we determined the noise affecting the propagating fronts.

The effective noise can be analysed [29] by considering the fluctuations of local velocities, *i.e.*, $\delta u(x,t) = u(x,t) - \overline{u}(t)$, with $u(x,t) \equiv [h(x,t+\tau) - h(x,t)]/\tau$. For convenience we considered in practice noise multiplied by the time scale used to determine the velocity, *i.e.*, the (scaled) noise amplitude used in the following is given by

$$\eta(x,t) = \delta h(x,t+\tau) - \delta h(x,t) \equiv \tau \delta u(x,t) \; . \tag{6.1}$$

We used this formulation since the camera system was moved in regular intervals and the actual value of the front height $\overline{h}(t)$ had to be estimated after the camera moves (see Chapter 4). We have used this scaled noise amplitude to estimate the amplitude distribution $P(\eta) \equiv N(\eta)/\sum_{\eta'} N(\eta')$ in the steady-state regime. Here $N(\eta)$ is the number of positions where η has the same value, and the sum goes over all values of η. Because of the temporal crossover behaviour, one has to analyse the effective noise below ($\tau < \tau_c$) and above ($\tau > \tau_c$) the crossover scale.

We showed [58, 57] that for short time steps the noise-amplitude distributions clearly have a power-law tail of the form

$$P(\eta) = c\, \eta^{-(\mu+1)}. \tag{6.2}$$

For the shortest time steps used, $\mu \simeq 1.7$ for the lens-paper [57] samples and $\mu \simeq 2.7$ for the two copier papers [58]. For increasing τ the power-law contributions in the tails of $P(\eta)$ became less visible, and the exponent μ increased towards $\mu \simeq 5$, around which value distributions became indistinguishable from Gaussian distributions. This latter behaviour was similar in all paper grades. There are also other factors which may contribute to the tails of the velocity-fluctuation distributions, such as skewness [59], but we do not consider these factors here.

Two-point correlation functions of the local velocity fluctuations $\delta u(x,t)$ were used to determine possible spatial and temporal correlations in the effective noise. Effective noise was found to be uncorrelated above the crossover scales r_c and t_c, which is in agreement with the asymptotic KPZ behaviour. Below the crossover scales we found the noise to be correlated in both space and time [58, 57], and the decay 'lengths' of these correlations seemed roughly to coincide with the crossover scales in the height-height correlation functions.

It thus, appears that the short-range correlations in the noise affecting the fronts, caused either by quenched noise or by correlated fluctuating disturbances, or both, are likely to be responsible for the crossovers and the related higher apparent exponents at short range. The continuous decay of short-range correlations

would also explain the lack of true scaling in that regime, *i.e.*, the running exponents do not show plateaux there.

6.3 Persistence

In order to determine the persistence properties, we chose to analyse the data for the $80\,\mathrm{g/m^2}$ copier paper since they have the best statistics. Figure 6.4 shows our experimental results for temporal and spatial persistence in the stationary state. It is evident that above the corresponding crossover scales, both these figures indicate agreement with the theoretical conjectures, $\theta_+^{\mathrm{temp}} = \theta_-^{\mathrm{temp}} = 1 - \beta$ and (roughly) $\theta_+^{\mathrm{spat}} = \theta_-^{\mathrm{spat}} = 1 - \chi$. No exact derivation of these exponents is available for KPZ systems. Below the crossover scales the data in Figure 6.4 show no real scaling, in analogy with the height-height correlation functions. We find no difference between the first-return distributions in the positive and negative directions since our distributions are normalised to one, and anisotropy does not appear in the plots.

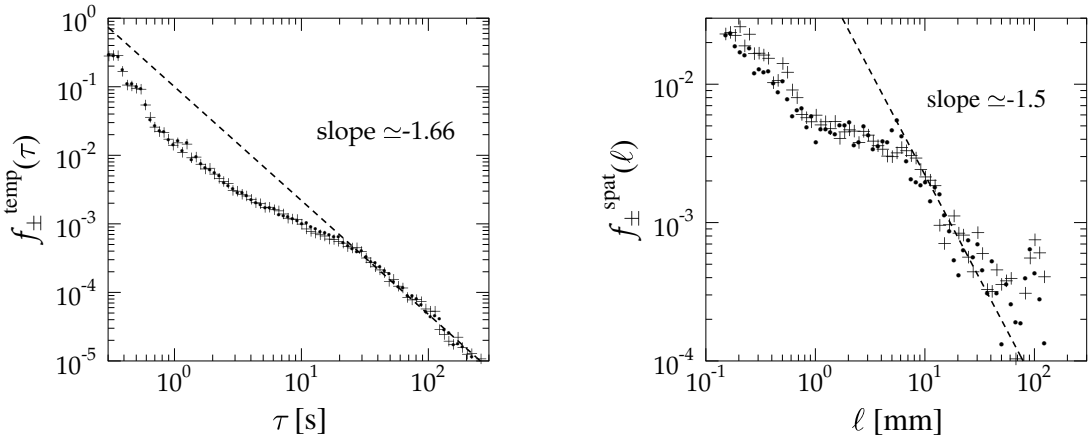

FIGURE 6.4 The stationary temporal (left) and spatial (right) first-return distributions. The dashed lines correspond to the asymptotic KPZ values of β and χ in Ref. [57], via the conjectures $f(\tau) \sim \tau^{-(2-\beta)}$ (temporal) and $f(\ell) \sim \ell^{-(2-\chi)}$ (spatial).

The expected persistence behaviour takes place only at long enough scales, where the physics is coarse-grained so as to obey the KPZ equation. There are effective correlations in the noise, with decay scales of a few seconds and a few millimetres [58]. In the short-range regime of the stationary state data, the spatial and temporal statistics are quite far from the scaling conjecture '$\theta = 1 - \beta$'. This agrees with the fact that the dynamics becomes Markovian only asymptotically. The short-range persistence does not result from an effectively stationary process that would differ from the long-range dynamics only by the fact that the height-height exponents are not defined. The deviation is greatest in the case of temporal behaviour, for which persistence decays slower than expected from the correlation function.

The first-return distributions for the transient regime of the dynamics are shown in Figure 4 in Ref. [55]. In our data the spatial long-range scaling turns out to be reminiscent of the stationary state. Also, there is no simple short range behaviour below the crossover scales. In some cases the short range scalings resemble power law ones, but the effective persistence exponents are never in agreement with those related to the decay of correlations. The spatial transient distribution, where the asymptotics are better defined, is given by $\ell^{-(2-\chi)}$ with $\chi = 1/2$ as in the saturated regime.

In principle, for a time window above the crossover time τ_c but below the saturation time some 'expected' (KPZ) temporal transient behaviour could be observed. However, the typically wide [57] crossover region around τ_c would interfere with it, unless the saturation time could be made long enough by, *e.g.*, considerably increasing the system size. Note that the up-down asymmetry [34] of the interface can be visible only for $\tau > \tau_c$ and $\ell > \ell_c$ [57].

6.4 Model parameters

6.4.1 Amplitudes, dimensionless constants and λ

The experimental determination of the universal amplitude ratios and the universal coupling constant (see Section 3.4.3) was slightly hampered by the presence of the crossover scales as, for these purposes, the correlation functions needed to be considered in the true scaling regime only. Despite the somewhat limited size of the scaling regime, the results are in rather good agreement with the theoretical predictions. In any case, correlation functions provide more accurate values for these quantities than the front widths, and we therefore used them here.

These quantities were augmented by an independent measurement of λ using the approach described in Section 3.4.1. The interface velocity was determined at each location with a time interval τ long enough to attain the KPZ regime, with a simultaneous determination of the local interface slope. The velocity versus slope data were then fitted by a parabola using slopes between -0.5 and 0.5, corresponding typically to about a half of all the slopes.

We determined the prefactors A and B of the spatial and temporal correlation functions, respectively, Eq. (3.15), from the measured correlation functions with χ and β fixed at $1/2$ and $1/3$. The values found in this way for A and B, and those for the other parameters, are shown in Table 6.3.

Combining the results for λ, A, and B with the exact KPZ exponents, we obtain for the coupling constant g^* and the universal amplitude ratio R_G the values shown in Table 6.3. Recalling that the mode-coupling value is $g^* \simeq 0.87$ [32], it is evident that the results are in good agreement with theory. If we use the measured exponents instead, g^* becomes 0.8(2), 0.8(2), and 2.7(4) for the $70\,\mathrm{g/m^2}$, $80\,\mathrm{g/m^2}$, and

TABLE 6.3 The correlation function amplitudes, λ and the universal R_G and g^* as extracted from the experimental data by using $\chi = 1/2$ and $\beta = 1/3$. [57]

Quantity	Paper grade		
	$70\,\mathrm{g/m^2}$	$80\,\mathrm{g/m^2}$	$9.1\,\mathrm{g/m^2}$
A	0.52(2)	0.475(7)	3.4(1)
B	0.186(12)	0.14(1)	8.0(8)
λ	0.465(2)	0.370(1)	4.0(4)
R_G	0.74(6)	0.73(5)	0.62(8)
g^*	0.79(9)	0.76(8)	1.0(2)

$9.1\,\mathrm{g/m^2}$ grades, respectively. The last value is due to the large effective β for the lens paper, caused by the very short saturated regime, and thereby poor statistics in the temporal correlation function. As the mode-coupling and simulation results for R_G vary in the range $R_G = 0.63 - 0.71$, agreement with theoretical predictions is good also in this case. Notice that (i) g^* and R_G are functionally related when the *exact* KPZ exponents are used in their expressions, and (ii) A (see Section 3.4.2) can be used as an independent estimate for the D/ν-ratio defined by the inverse method (see Section 3.5.1) for which results are shown in the next section.

Although the interface width could not be used to obtain an estimate for the asymptotic surface width amplitude C_t used in Eq. (3.18) and, thereby, for the R, the local width allows for the determination of the universal scaling function from the experimental data as described in Section 2.3. On can show [2,3] that

$$w(\ell, t) = C_\ell \ell^\chi F\left(\frac{|\lambda| C_\ell t}{\ell^z}\right) , \tag{6.3}$$

where C_ℓ is determined from the asymptotic value $w(\ell, t = \infty) = C_\ell \ell^\chi$. Using a maximum value of $\ell \simeq 14\,\mathrm{cm}$, and fitting the C_ℓ values for the three grades, one can collapse the time-dependent data with the aid of the λ values as measured from the slope-dependent local velocities [2,3]. The result is shown in Figure 12 in Ref. [57]. As the measured λ and C_ℓ values are not very accurate, we show in the inset of this figure the best collapse of the data achieved using C_ℓ essentially as a free parameter.

6.4.2 KPZ and its parameters by inversion from observed fronts

We have verified the KPZ equation and determined its effective coefficients using the inverse method (see Section 3.5.1) and independent estimates for c and λ were obtained using the slope-dependent velocity (see Section 3.4.1). The results are shown in Table 6.4 for the $80\,\mathrm{g/m^2}$ copier and the $9.1\,\mathrm{g/m^2}$ lens paper grades, and magnetic flux fronts penetrating a thin-film high-T_c superconductor [51]. The

TABLE 6.4 Measured average values for KPZ coeffients and the ratio D/ν. For the slow-combustion fronts $l = 11.6 \ldots 17.6\,\mathrm{mm}$ and $\tau = 0.4\,\mathrm{s}$, and for the magnetic flux fronts $l = 11.2 \ldots 19.6\,\mu\mathrm{m}$ and $\tau = 0.5\,\mathrm{s}$, were used as the coarse-graining scales for c and λ. The scaled ν and the D/ν ratio were determined for $\ell = 17.5\,\mathrm{mm}$ and $\tau = 25.6\,\mathrm{s}$ (copier-paper), and $\ell = 17.6\,\mathrm{mm}$ and $\tau = 1.6\,\mathrm{s}$ (lens-paper). The D/ν ratio for the magnetic flux was determined for $\ell = 22.4\,\mu\mathrm{m}$ and $\tau = 3.5\,\mathrm{s}$.

Coefficient	Inverse method			Slope-dependent velocity		
	Copier	Lens	Flux $\times 10^{-3}$	Copier	Lens	Flux $\times 10^{-3}$
$c\,[\mathrm{mm/s}]$	0.49(2)	9.2(5)	27.0(1)	0.485(2)	9.1(2)	27.1(2)
$\lambda\,[\mathrm{mm/s}]$	0.40(2)	4.1(2)	15.9(8)	0.37(3)	5.1(2)	17.4(2)
$\nu\left(\frac{\tau}{\Delta t}\right)^{-1/3}\,[\mathrm{mm^2/s}]$	0.049(3)	2.0(1)	–	–	–	–
$D/\nu\,[\mathrm{mm}]$	0.83(5)	4.6(1.1)	6(3)	–	–	–

behaviour of the coefficients and the D/ν-ratio as functions of coarse graining is displayed for the $80\,\mathrm{g/m^2}$ copier paper in Figures 6.5 and 6.6.

We have also tested the inverse method for non-KPZ equation by including higher-order terms with related coefficients, and comparing the results with those from numerical simulations of a discrete KPZ equation with real noise as determined by optical scans of lens-paper samples. It appears that the inverse method finds it difficult to distinguish, *e.g.*, a fourth-order derivative from noise, while the other KPZ parameters seemed to be more or less unaffected by inclusion of this term. On the other hand, the data produced by KPZ simulations with real noise gave as well rise to a non-zero fourth-order derivative when the inverse method was applied to these data. Also, the coefficient of the fourth-order derivative was higher for the simulated data than for the measured data. In this sense we can conclude that no evidence was found for the existence (asymptotically) of higher-order terms in the equation of motion for the measured fronts.

The parabolic dependence of the local front velocity on the local slope of the front provides fairly direct independent evidence of the existence of a KPZ type nonlinear term in the evolution equation. Furthermore, higher-order polynomial fits to the slope-dependent front velocity of the lens-paper fronts lend some support to a square-root form of the slope dependence, expected when driving is along the local normal. This shows up at short length scales, asymptotically the higher-order terms are irrelevant.

The estimates for the zero-slope velocity c and the nonlinear term λ could be determined using both of the above mentioned methods, and they were in good agreement with each others. The estimates for the ratio D/ν of the noise correlator D and the 'surface tension' ν were obtained using the inverse method. For slow

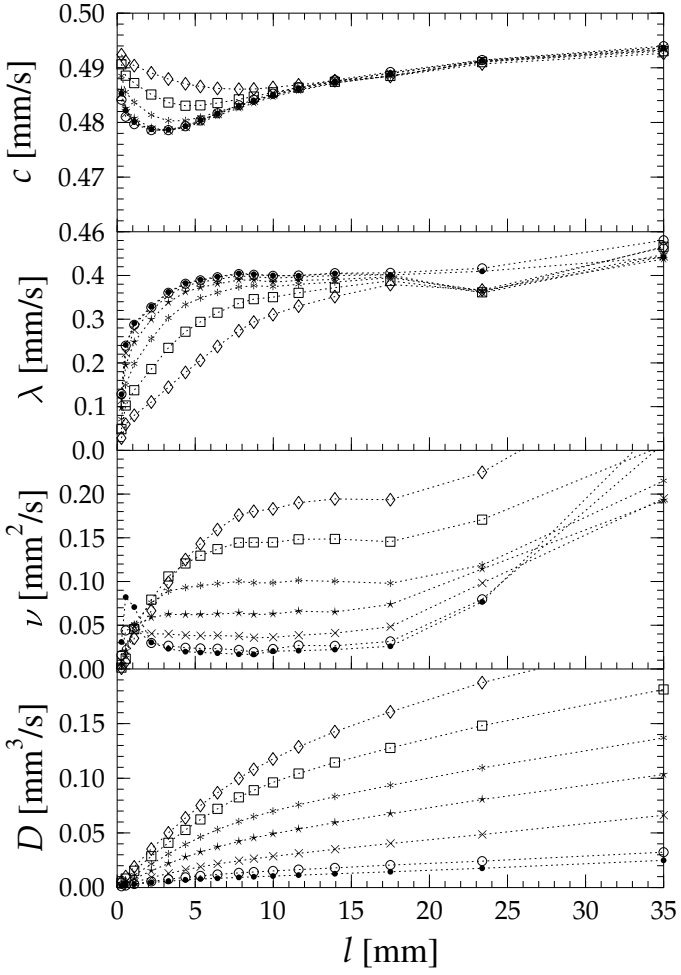

FIGURE 6.5 Model parameters c, λ, ν and D determined by the inverse method and averaged over 18 burns of the $80\,\mathrm{g/m^2}$ copier-paper, as functions of the cutoff length ℓ for $\tau = 0.4\,(\cdot)\,\ldots\,25.6\,(\diamond)\,\mathrm{s}$.

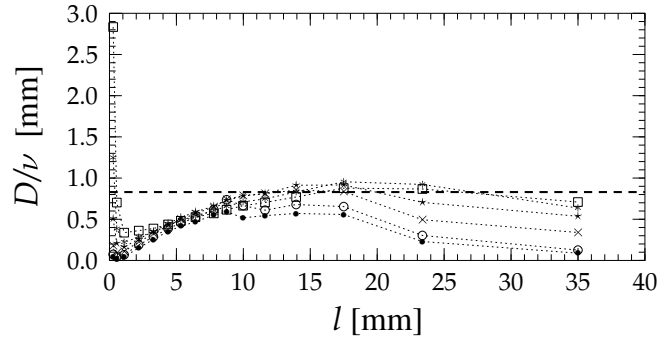

FIGURE 6.6 Measured D/ν as a function of cutoff length ℓ for the $80\,\mathrm{g/m^2}$ copier-paper burns.

combustion fronts the D/ν thus obtained could be compared with a previous result [57] for the asymptotic amplitude of the spatial height-height correlation function, $A = D/\nu$, shown in Table 6.3 with again good agreement. In all cases this ratio was found to converge quite well for increasing coarse-graining scales ℓ and τ. For ν a τ-dependent scaling form was determined for the slow-combustion fronts.

For the magnetic flux fronts the values were obtained by averaging over 9 sets of fronts measured on the same sample. The inverse method and the system size set an upper limit for the feasible coarse-graining length for the used sets of fronts, which is somewhat smaller than he crossover length estimated from the spatial height-height correlation function in Ref. [69]. Since all nine measurements were made on the same sample, noise averaging (over structural defects in the sample) was less extensive than for the slow combustion fronts, and saturation of the parameter values was not quite as good. Both c and λ were also estimated using the slope-dependent approach, and we think the values by the inverse method are however fairly reliable as they are consistent with the other estimates.

Chapter 7

Conclusions

The main result of our experimental work was to demonstrate in detail that asymptotically the scaling behaviour of slow-combustion fronts are consistent with those of the Kardar-Parisi-Zhang equation with uncorrelated Gaussian noise. To achieve this result extensive averaging over noise turned out to be necessary. This is of course something one should realize already on theoretical grounds, but apparently had not been sufficiently appreciated earlier.

The scaling properties of this system were analysed perhaps in more detail than those of any other single experimental non-equilibrium system before. In addition to the typical scaling exponents, the strong-coupling fixed point, a universal amplitude ratio, and an estimate of the scaling function of the local interface width, were also determined. By an inverse method, and also from the slope-dependent local velocity of the fronts, basically all the parameters of the KPZ equation applicable to slow-combustion fronts were determined, specific of course to the three grades of paper used in the samples. Indication was also found for higher order terms not being relevant in the proper Langevin equation, but no definite conclusions could be drawn.

Having firmly established that the system indeed displays KPZ dynamics, we then proceeded to analyse the persistence properties of front-height fluctuations. In the KPZ case, the theoretical results for these fluctuations are somewhat less certain than the scaling properties described above. We could show again that, asymptotically, persistence of stationary height fluctuations display well defined scaling behaviour, temporal as well as spatial fluctuations, with scaling exponents in agreement with the respective conjectures for the KPZ universality class. Results were also obtained for the transient persistence, especially of the spatial height fluctuations. These results will hopefully motivate future theoretical work in this area.

In all the quantities analysed so far, the asymptotic KPZ scaling was preceded by crossover from a different kind of short-range behaviour. Running-exponent analysis of this short-range behaviour revealed that, at least within the present experimental accuracy, there is no true scaling regime at short scales. In log-log scale even the short-range parts of *e.g.* height-height correlation functions looked how-

ever fairly linear, and linear fits of them provided apparent scaling exponents typically much higher than the corresponding KPZ exponents. The short-range parts of the correlation functions also displayed apparent 'multiscaling'. The persistence properties of the front-height fluctuations indicate in particular that the stochastic process behind the short-range behaviour is non-Markovian.

The reason for the observed short-range behaviour could be traced down to the properties of effective noise. This noise was measured from the velocity fluctuations of the fronts, and was found to have short-range spatial and temporal correlations, as well as a power-law tail in its amplitude distribution at short time scales. The decay rates of the correlations, and the disappearance of the non-trivial amplitude distribution, were all approximately related to the observed crossover lengths and times from the short-range regime to the asymptotic KPZ regime. The spatial crossover scale seems to be mainly related to, but not completely determined by, the structural disorder in the samples. The temporal crossover on the other hand seems to be clearly affected by dynamical effects, as it was typically much longer than one would expect from the spatial crossover length and the front velocity. The non-trivial amplitude distribution and apparent multiscaling appear to completely arise from dynamical effects.

The effective noise thus gives rise to a new time and a new length scale, the crossover scales, in the behaviour of the fronts, and these additional scales must properly be taken into account when analysing the scaling properties of the fronts. We would expect similar features to arise quite naturally in all experimental systems. It may well be that the large variation in the experimental scaling exponents is partly related to this feature, in addition to possible inadequacies in noise averaging. It is also evident that our theoretical understanding of stochastic processes which are non-Markovian at short time and length scales, but are Markovian asymptotically, is still very rudimentary.

Bibliography

[1] ALBERT, R., BARABÁSI, A.-L., CARLE, N., AND DOUGHERTY, A., *Driven Interfaces in Disordered Media: Determination of Universality Classes from Experimental Data*. Phys. Rev. Lett. **81** (1998) 2926–2929.

[2] AMAR, J. G. AND FAMILY, F., *Universal Scaling Function and Amplitude Ratios in Surface Growth*. Phys. Rev. A **45** (1992) R3373–R3376.

[3] AMAR, J. G. AND FAMILY, F., *Universality in Surface Growth: Scaling Functions and Amplitude Ratios*. Phys. Rev. A **45** (1992) 5378–5393.

[4] AMARAL, L. A. N., BARABÁSI, A.-L., MAKSE, H. A., AND STANLEY, H. E., *Scaling Properties of Driven Interfaces in Disordered Media*. Phys. Rev. E **52** (1995) 4087–4104.

[5] AMARAL, L. A. N., BARABÁSI, A.-L., AND STANLEY, H. E., *Universality Classes for Interface Growth with Quenched Disorder*. Phys. Rev. Lett. **73** (1994) 62–65.

[6] AMARAL, L. A. N. AND MAKSE, H. A., *Comment on "Kinetic Roughening in Slow Combustion of Paper"*. Phys. Rev. Lett. **80** (1998) 5706.

[7] BALANKIN, A. S. AND MATAMOROS, D. M., *Unconventional Anomalous Roughening in the Slow Combustion of Paper*. Phil. Mag. Lett. **81** (2001) 495–503.

[8] BARABÁSI, A.-L., BOURBONNAIS, R., JENSEN, M., KERTÉSZ, J., VICSEK, T., AND ZHANG, Y.-C., *Multifractality of Growing Surfaces*. Phys. Rev. A **45** (1992) R6951–R6954.

[9] BARABÁSI, A.-L. AND STANLEY, H. E., *Fractal Concepts in Surface Growth* (Cambridge University Press, Cambridge, UK, 1995).

[10] BARABÁSI, A.-L., SZÉPFALUSY, P., AND VICSEK, T., *Multifractal Spectra of Multi-Affine Functions*. Physica A **178** (1991) 17–28.

[11] BARABÁSI, A.-L. AND VICSEK, T., *Multifractality of Self-Affine Fractals*. Phys. Rev. A **44** (1991) 2730–2733.

[12] BUCETA, J., PASTOR, J., RUBIO, M. A., AND DE LA RUBIA, F. J., *Finite Resolution Effects in the Analysis of the Scaling Behavior of Rough Surfaces*. Phys. Rev. E **61** (2000) 6015–6018.

[13] BULDYREV, S. V., HAVLIN, S., KERTÉSZ, J., STANLEY, H. E., AND VICSEK, T., *Ballistic Deposition with Power-Law Noise: A Variant of the Zhang Model*. Phys. Rev. A **43** (1991) 7113–7116.

[14] DEKER, U. AND HAAKE, F., *Fluctuation-Dissipation Theorems for Classical Processes*. Phys. Rev. A **11** (1975) 2043–2056.

[15] DING, M. AND YANG, W., *Distribution of the First Return Time in Fractional Brownian Motion and its Applications to the Study of On-Off Intermittency*. Phys. Rev. E **52** (1995) 207–213.

[16] EDWARDS, S. F. AND WILKINSON, D. R., *The Surface Statistics of a Granular Aggregate*. Proc. R. Soc. London, Ser. A **381** (1982) 17–31.

[17] EKELAND, I. AND TEMAM, R., *Convex Analysis and Variational Problems*, vol. 1 of *Studies in Mathematics and its Applications* (North-Holland, Amsterdam, 1976).

[18] FAMILY, F. AND VICSEK, T., *Scaling of the Active Zone in the Eden Process on Percolation Networks and the Ballistic Deposition Model*. J. Phys. A **18** (1985) L75–L81.

[19] FORREST, B. M. AND TANG, L.-H., *Surface Roughening in a Hypercube-Stacking Model*. Phys. Rev. Lett. **64** (1990) 1405–1408.

[20] GIACOMETTI, A. AND ROSSI, M., *Pseudospectral Approach to Inverse Problem in Interface Dynamics*. Phys. Rev. E **63** (2001) 046102. `cond-mat/0012178`.

[21] GIADA, L., GIACOMETTI, A., AND ROSSI, M., *Pseudospectral Method for the Kardar-Parisi-Zhang Equation*. Phys. Rev. E **65** (2002) 036134. `cond-mat/0112333`.

[22] GLOWINSKI, R. AND KÄRKKÄINEN, T., *Nonsmooth Successive Overrelaxation Method for Robust Restoration of Smooth Images*. In preparation.

[23] GONZALEZ, R. AND WOODS, R., *Digital Image Processing* (Addison-Wesley, 1993).

[24] GWA, L.-H. AND SPOHN, H., *Bethe Solution for the Dynamical-Scaling Exponent of the Noisy Burgers Equation*. Phys. Rev. A **46** (1992) 844–854.

[25] GWA, L.-H. AND SPOHN, H., *Six-Vertex Model, Roughened Surfaces, and an Asymmetric Spin Hamilton*. Phys. Rev. Lett. **68** (1992) 725–728.

[26] HALPIN-HEALY, T. AND ZHANG, Y.-C., *Kinetic Roughening Phenomena, Stochastic Growth, Directed Polymers and all that*. Phys. Rep. **254** (1995) 215–415.

[27] HANSEN, A., ENGØY, T., AND MÅLØY, K. J., *Measuring Hurst Exponents with the First Return Method*. Fractals **2** (1994) 527–533.

[28] HE, S., KAHANDA, G. L. M. K. S., AND WONG, P.-Z., *Roughness of Wetting Fluid Invasion Fronts in Porous Media*. Phys. Rev. Lett. **69** (1992) 3731–3734.

[29] HORVÁTH, V. K., FAMILY, F., AND VICSEK, T., *Anomalous Noise Distribution of the Interface in Two-Phase Fluid Flow*. Phys. Rev. Lett. **67** (1991) 3207–3210.

[30] HORVÁTH, V. K., FAMILY, F., AND VICSEK, T., *Dynamic Scaling of the Interface in Two-Phase Viscous Flows in Porous Media*. J. Phys. A **24** (1991) L25–L29.

[31] HUBER, P. J., *Robust Statistics*, Wiley series in Probability and Mathematical Statistics (John Wiley & Sons, New York, 1981).

[32] HWA, T. AND FREY, E., *Exact Scaling Function of Interface Growth Dynamics*. Phys. Rev. A **44** (1991) R7873–R7876.

[33] KAHANDA, G. L. M. K. S., ZOU, X.-Q., FARRELL, R., AND WONG, P.-Z., *Columnar Growth and Kinetic Roughening in Electrochemical Deposition*. Phys. Rev. Lett. **68** (1992) 3741–3744.

[34] KALLABIS, H. AND KRUG, J., *Persistence of Kardar-Parisi-Zhang Interface*. Europhys. Lett. **45** (1999) 20–25.

[35] KARDAR, M., PARISI, G., AND ZHANG, Y.-C., *Dynamic Scaling of Growing Interfaces*. Phys. Rev. Lett. **56** (1986) 889–892.

[36] KERTÉSZ, J. AND WOLF, D. E., *Noise Reduction in Eden Models: II. Surface Structure and Intrinsic Width*. J. Phys. A **21** (1988) 747–761.

[37] KRÍZEK, M. AND NEITTAANMÄKI, P., *Finite Element Approximation of Variational Problems and Applications*, vol. 50 of *Pitman Monographs and Surveys in Pure and Applied Mathematics* (Longman Scientific & Technical, Essex, England, 1990).

[38] KRUG, J., *Kinetic Roughening by Exceptional Fluctuations*. J. Phys. I **1** (1991) 9–12.

[39] KRUG, J., KALLABIS, H., MAJUMDAR, S. N., CORNELL, S. J., BRAY, A. J., AND SIRE, C., *Persistence Exponents for Fluctuating Interfaces*. Phys. Rev. E **56** (1997) 2702–2712. `cond-mat/9704238`.

[40] KRUG, J., MEAKIN, P., AND HALPIN-HEALY, T., *Amplitude Universality for Driven Interfaces and Directed Polymers in Random Media*. Phys. Rev. A **45** (1992) 638–653.

[41] LAM, C.-H. AND SANDER, L. M., *Inverse Method for Interface Problems*. Phys. Rev. Lett. **71** (1993) 561–564.

[42] LESCHHORN, H., *Anisotropic Interface Depinning: Numerical Results*. Phys. Rev. E **54** (1996) 1313–1320.

[43] LESCHHORN, H., NATTERMANN, T., STEPANOW, S., AND TANG, L.-H., *Driven Interface Depinning in a Disorderd Medium*. Ann. Phys. (Leipzig) **6** (1997) 1–34. `cond-mat/9603114`.

[44] MAJUMDAR, S. N., *Persistence in Nonequilibrium Systems*. Curr. Sci. **77** (1999) 370–375. `cond-mat/9907407`.

[45] MAJUMDAR, S. N. AND BRAY, A. J., *Spatial Persistence of Fluctuating Interfaces*. Phys. Rev. Lett. **86** (2001) 3700–3703. `cond-mat/0009439`.

[46] MAJUMDAR, S. N., BRAY, A. J., CORNELL, S. J., AND SIRE, C., *Global Persistence Exponent for Nonequilibrium Critical Dynamics*. Phys. Rev. Lett. **77** (1996) 3704–3707. `cond-mat/9606123`.

[47] MAJUMDAR, S. N., BRAY, A. J., AND EHRHARDT, G. C. M. A., *Persistence of a Continuous Stochastic Process with Discrete-Time Sampling*. Phys. Rev. E **64** (2001) 015101(R). `cond-mat/0011290`.

[48] MÄKELÄ, M. M. AND NEITTAANMÄKI, P., *Nonsmooth Optimization. Analysis and Algorithms with Applications to Optimal Control* (World Scientific, Singapore, 1992).

[49] MASLOV, S., PACZUSKI, M., AND BAK, P., *Avalanches and 1/f Noise in Evolution and Growth Models*. Phys. Rev. Lett. **73** (1994) 2162–2165.

[50] MAUNUKSELA, J., MYLLYS, M., KÄHKÖNEN, O.-P., TIMONEN, J., PROVATAS, N., ALAVA, M. J., AND ALA-NISSILA, T., *Kinetic Roughening in Slow Combustion of Paper*. Phys. Rev. Lett. **79** (1997) 1515–1518.

[51] MAUNUKSELA, J., MYLLYS, M., MERIKOSKI, J., KÄRKKÄINEN, T., TIMONEN, J., WELLING, M. S., AND WIJNGAARDEN, R. J., *Determination of the Stochastic Evolution Equation from Noisy Experimental Data* (2003). To appear in *Eur. Phys. J. B*.

[52] MEAKIN, P., *Fractals, Scaling and Growth Far From Equilibrium* (Cambridge University Press, Cambridge, UK, 1998).

[53] MEAKIN, P., *Fractals, Scaling and Growth Far From Equilibrium* (Cambridge University Press, 1998), pp. 130–135.

[54] MEDINA, E., HWA, T., KARDAR, M., AND ZHANG, Y.-C., *Burgers Equation with Correlated Noise: Renormalization-Group Analysis and Applications to Directed Polymers and Interface Growth*. Phys. Rev. A **39** (1989) 3053–3075.

[55] MERIKOSKI, J., MAUNUKSELA, J., MYLLYS, M., TIMONEN, J., AND ALAVA, M. J., *Temporal and Spatial Persistence of Combustion Fronts in Paper*. Phys. Rev. Lett. **90** (2003) 024501. `cond-mat/0203428`.

[56] MYLLYS, M., *Experimental Realization of KPZ Dynamics: Slow Combustion of Paper*. PhD thesis, In preparation.

[57] MYLLYS, M., MAUNUKSELA, J., ALAVA, M., ALA-NISSILA, T., MERIKOSKI, J., AND TIMONEN, J., *Kinetic Roughening in Slow Combustion of Paper*. Phys. Rev. E **64** (2001) 036101. `cond-mat/0105234`.

[58] MYLLYS, M., MAUNUKSELA, J., ALAVA, M. J., ALA-NISSILA, T., AND TIMONEN, J., *Scaling and Noise in Slow Combustion of Paper*. Phys. Rev. Lett. **84** (2000) 1946–1949.

[59] NEERGARD, J. AND DEN NIJS, M., *Stationary-State Skewness in KPZ-Type Growth*. J. Phys. A **30** (1997) 1935–1952. `cond-mat/9610189`.

[60] NOCEDAL, J. AND WRIGHT, S. J., *Numerical Optimization* (Springer, New York, 1999).

[61] PRÄHOFER, M. AND SPOHN, H., *Current fluctuations for the totally asymmetric simple exclusion process*, in *In and out of equilibrium*, edited by V. Sidoravicius (Birkhauser Boston, 2002), vol. 51 of *Progress in Probability*, pp. 185–204. `cond-mat/0101200`.

[62] PRÄHOFER, M. AND SPOHN, H., *Scale Invariance of the PNG Droplet and the Airy Process*. J. Stat. Phys. **108** (2002) 1071–1106. `math.PR/0105240`.

[63] PROVATAS, N., ALA-NISSILA, T., GRANT, M., ELDER, K. R., AND PICHÉ, L., *Flame Propagation in Random Media*. Phys. Rev. E **51** (1995) 4232–4236. `cond-mat/9405040`.

[64] PROVATAS, N., ALA-NISSILA, T., GRANT, M., ELDER, K. R., AND PICHÉ, L., *Scaling, Propagation, and Kinetic Roughening of Flame Fronts in Random Media*. J. Stat. Phys. **81** (1995) 737–759. `cond-mat/9506017`.

[65] RAO, C. R., *Methodology Based on the L_1-Norm, in Statistical Inference*. The Indian Journal of Statistics **50** (1988) 289–313.

[66] RUBIO, M. A., EDWARDS, C. A., DOUGHERTY, A., AND GOLLUB, J. P., *Self-Affine Fractals Interfaces from Immiscible Displacement in Porous Media*. Phys. Rev. Lett. **63** (1989) 1685–1688.

[67] SCHMITTBUHL, J., VILOTTE, J.-P., AND ROUX, S., *Reliability of Self-Affine Measurements*. Phys. Rev. E **51** (1995) 131–147.

[68] SIEGERT, M., *Determining Exponents in Models of Kinetic Surface Roughening*. Phys. Rev. E **53** (1996) 3209–3214.

[69] SURDEANU, R., WIJNGAARDEN, R. J., VISSER, E., HUIJBREGTSE, J. M., RECTOR, J. H., DAM, B., AND GRIESSEN, R., *Kinetic Roughening of Penetrating Flux Fronts in High-T_c Thin Film Superconductors*. Phys. Rev. Lett. **83** (1999) 2054–2057.

[70] TANG, L.-H. AND LESCHHORN, H., *Pinning by Directed Percolation*. Phys. Rev. A **45** (1992) R8309–R8312.

[71] VICSEK, T., *Fractal Growth Phenomena* (World Scientific, Singapore, 1992), 2nd ed.

[72] VICSEK, T., CSERZŐ, M., AND HORVÁTH, V. K., *Self-Affine Growth of Bacterial Colonies*. Physica A **167** (1990) 315–321.

[73] WOLF, D. E. AND KERTESZ, J., *Noise Reduction in Eden Models: I*. J. Phys. A **20** (1987) L257–L261.

[74] ZHANG, J., ZHANG, Y.-C., ALSTRØM, P., AND LEVINSEN, M. T., *Modeling Forest Fire by a Paper-Burning Experiment, a Realization of the Interface Growth Mechanism*. Physica A **189** (1992) 383–389.

[75] ZHANG, Y.-C., *Non-Universal Roughening of Kinetic Self-Affine Interfaces*. J. Phys. France **51** (1990) 2129–2134.